3

Structures of Cytochrome P450 Enzymes

Thomas L. Poulos and Eric F. Johnson

1. Introduction

Much of what we know about the molecular level structure–function relationships in P450s is based on studies with the camphor monooxygenase system from *Pseudomonas putida*. Given that P450cam was the first P450 to be purified in sufficient quantities for structure–function relationships, it is not too surprising that P450cam was the first P450 crystal structure to be solved. The high-resolution structure of P450cam was published in 1987[1], and remained the paradigm for P450 structure–function studies until the P450BM3 structure was solved in 1993[2]. Since then the rate at which new P450 structures are being solved has increased dramatically and at present there are structures for 20 unique P450s on deposit in the Protein Data Bank with others waiting in the wings. Some of the new advances that have been made since the last edition of this book are the structures of other redox components of P450 monooxygenase systems, of the first electron transfer complex, of new substrate complexes, of the first P450s from thermophilic organisms, and of the first membrane-bound P450. In the present chapter, we summarize some of these more important recent findings with full recognition that the P450 structural field is moving much more quickly than in the time frame of previous editions of this book. As a result, the current chapter must be considered a snapshot in time on where we now stand in P450 crystallography.

2. Overall Architecture

There are now a sufficient number of structures to safely state that the overall P450 fold is quite conservative. Perhaps more surprising is that the P450 fold is unique and despite the many new structures that have been solved since P450cam, no non-P450 structure has yet been found to share the P450 fold. Thus, the P450 fold appears to be uniquely adapted for the heme-thiolate chemistry required for oxygen activation, the binding of redox partners, and the stereochemical requirements of substrate recognition.

The structures of several P450s are shown in Figure 3.1, while Figure 3.2 highlights some of the key secondary structural elements. Although the overall fold is maintained, the precise positioning of various structural elements differs substantially. In general, the closer to the heme, the more conserved the structure, especially helices I and L, which directly contact the heme. As expected, those regions controlling substrate specificity differ the most, especially the B′ helix. For example, in P450eryF, the B′ helix is oriented about 90° from the orientation observed in P450cam. The

Thomas L. Poulos • Department of Molecular Biology and Biochemistry and the Program in Macromolecular Structure, University of California, Irvine, Irvine, CA. **Eric F. Johnson** • Department of Molecular and Experimental Medicine, The Scripps Research Institute, La Jolla, CA.

Cytochrome P450: Structure, Mechanism, and Biochemistry, 3e, edited by Paul R. Ortiz de Montellano Kluwer Academic / Plenum Publishers, New York, 2005.

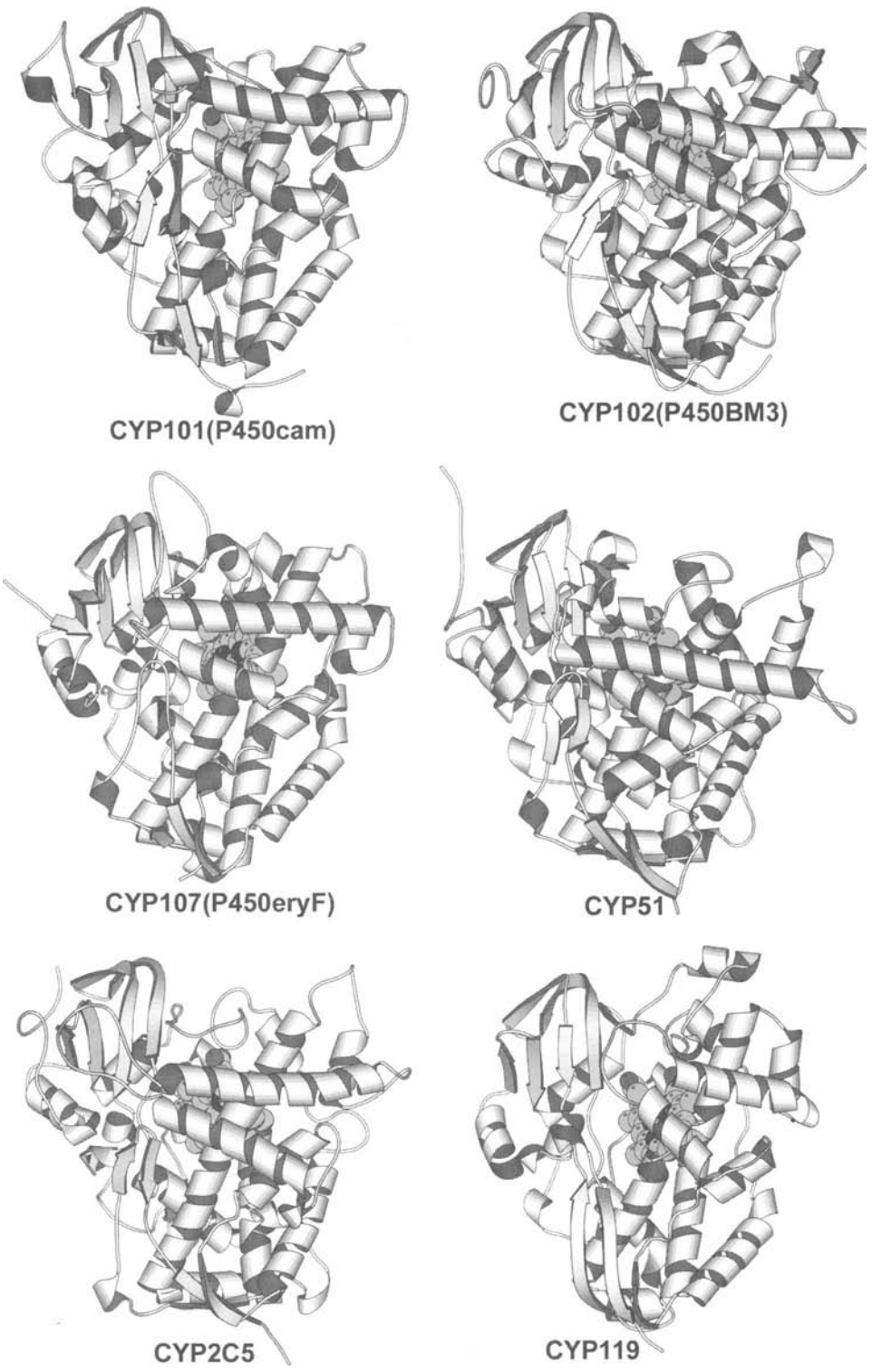

Figure 3.1. A representative example of known P450 structures illustrating the common three-dimensional fold.

Figure 3.2. The structure of P450cam with key helical segments labeled.

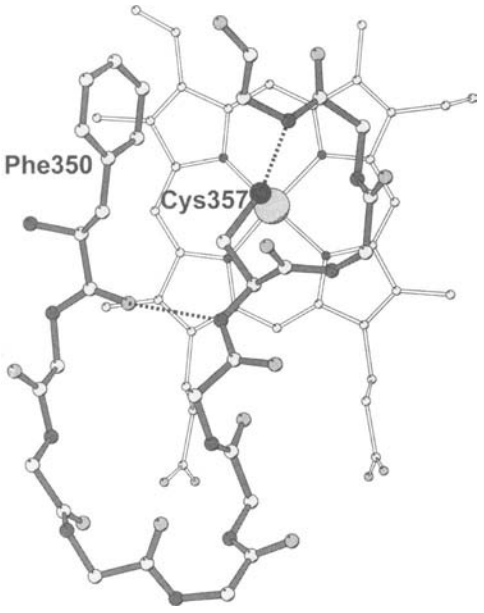

Figure 3.3. The Cys ligand "loop" in P450cam. The dashed lines indicate key hydrogen bonding interactions that aid in stabilizing the Cys ligand.

effect is a substantial change in local environment that is required for substrate selectivity.

Not too surprisingly, the most conserved elements of the P450 structure center on the heme-thiolate oxygen activation chemistry. The most noteworthy is the β-bulge segment housing the Cys ligand (Figure 3.3), just prior to the L helix. This rigid architecture is required to both protect the Cys ligand and hold it in place in order to accept H-bonds from peptide NH groups. This arrangement is not only found in all P450s but in two closely related proteins, nitric oxide synthase (NOS) and chloroperoxidase (CPO). Both NOS and CPO are heme-thiolate enzymes and like P450s catalyze monooxygenation reactions. Exactly as in P450, the Cys ligand in CPO accepts H-bonds from peptide NH groups[3]. NOS is similar except that one of the H-bonds is provided by the indole ring N atom of a conserved Trp residue[4–6]. Such an H-bonding arrangement is not unique to heme thiolate proteins but is a characteristic feature of proteins containing Cys–Fe ligation and was first observed in the ferredoxins[7]. These H-bonds aid in regulating the heme iron redox potential[8, 9]. Without such H-bonds, the redox potential would be too low for reduction by redox partners. Thus, it appears that the protein must provide a suitable electrostatic environment around the Cys ligand in order to maintain the redox potential in a physiologically accessible range. The same is true for a close cousin to P450, the peroxidases. Here His serves as the axial ligand, but in this case, it is necessary to decrease rather than increase the redox potential[10]. As a result, the His ligand H-bonds with a buried Asp residue which imparts greater imidazolate character to the His thus lowering the heme iron redox potential[11–15].

The other highly conserved region involved in O_2 activation is the portion of helix I near the heme Fe (Figure 3.4). Thr252 is involved in a local helical distortion in P450cam such that the Thr side chain OH donates an H-bond to a peptide carbonyl oxygen that would normally be involved in an α-helical H-bond. This Thr is not strictly conserved. For example, P450eryF contains Ala instead of Thr (Figure 3.4). Even so, P450eryF also exhibits a similar distortion in the I helix. In addition, a water molecule in P450eryF takes the place of the Thr side chain OH thus maintaining a very similar H-bonding pattern. This arrangement is thought to be quite important in the proper delivery of protons to the iron-linked oxygen required for cleavage of the O–O bond thus generating the active Fe–O hydroxylating species. The growing consensus is that ordered solvent at the active site serves as the direct proton donor to the iron-linked dioxygen[16, 17]. The most revealing crystal structures that support this view are the P450cam–oxy complex[18] and resting state ferric P450eryF[19]. In the P450cam–oxy

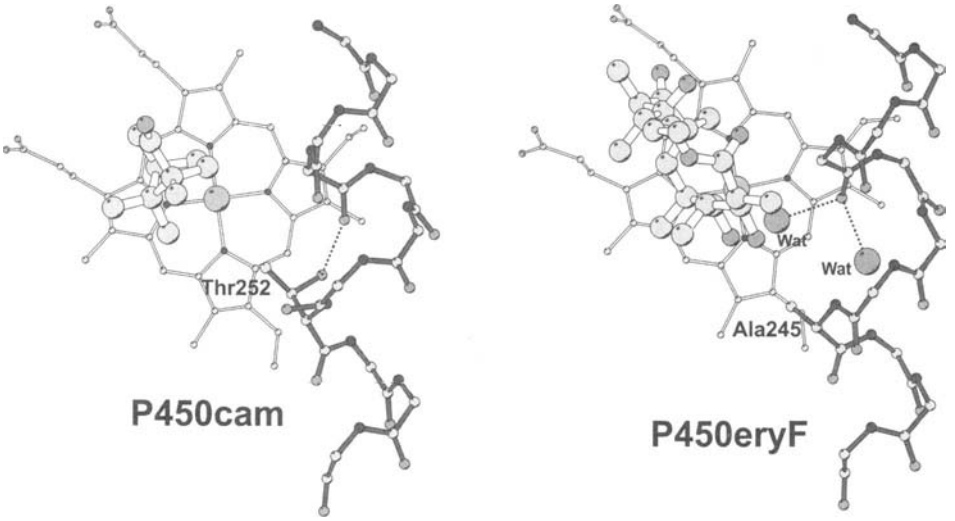

Figure 3.4. A comparison of the I helix region in P450cam and P450eryF. The large gray spheres indicate water molecules that complete the hydrogen bonding network in P450eryF.

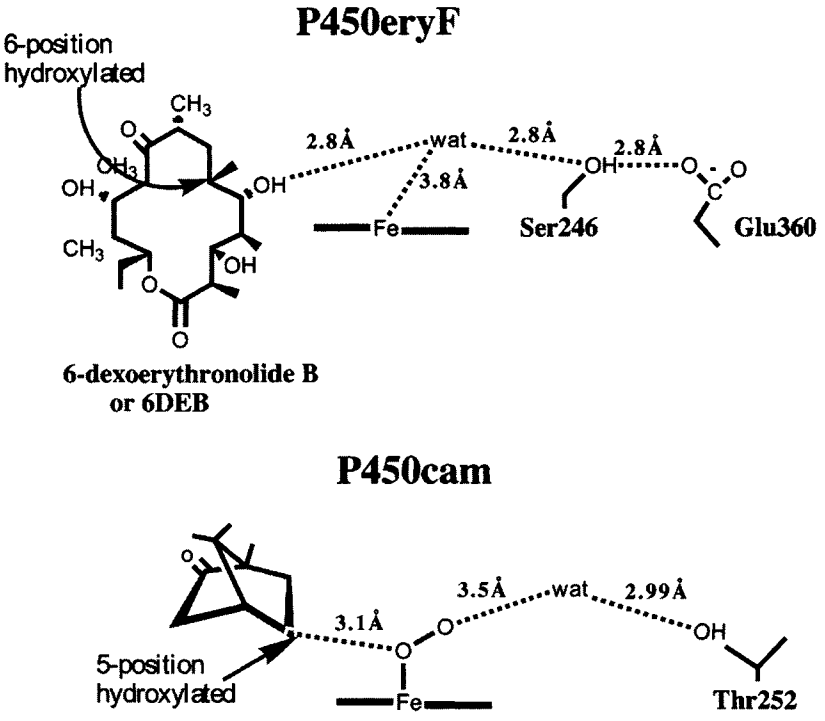

Figure 3.5. A comparison of the solvent-mediated hydrogen bonding network in P450eryF and the oxy-complex of P450cam[18]. In both cases, a critically positioned water molecule very likely serves as the proton donor to bound dioxygen.

complex, two new waters are found in the active site, one of which is shown in Figure 3.5. This new water is close to dioxygen and may participate in relaying protons to dioxygen. P450eryF also has a water similarly positioned (Figure 3.5). P450eryF, however, uses a substrate-assisted mechanism since a substrate OH anchors the key water in place via H-bonding. While the details of the proton shuttle machinery may differ from one P450 to the next, the surrounding protein groups and, in at least one case, the substrate, generally position solvent in the active site for proton delivery to dioxygen resulting in cleavage of the O–O bond.

3. P450s from Thermophiles

Given that P450s are found in such a wide variety of organisms, it is not surprising that P450s also are found in thermophiles. The first to be discovered was CYP119 from the acidothermophilic archaeon *Sulfolobus solfataricus*[20]. Subsequent cloning and expression showed that CYP119 melts near 90 °C compared to P450cam which melts near 50°C[21]. The crystal structure of CYP119 was first solved by Yano *et al.*[22] followed by an independent structure determination by Park *et al.*[23]. The most notable difference between CYP119 and other P450s is that CYP119 is much smaller, consisting of only 368 residues. The difference in size is primarily due to a shorter N-terminal segment and shorter surface loops. A unique clustering of aromatic residues running down one side of the molecule (Figure 3.6) is thought to be the structural basis for thermal stability. Mutating one of these residues, Phe24, to Ser lowers the melting temperature about 10°C[23]. A more extensive mutagenesis analysis of the

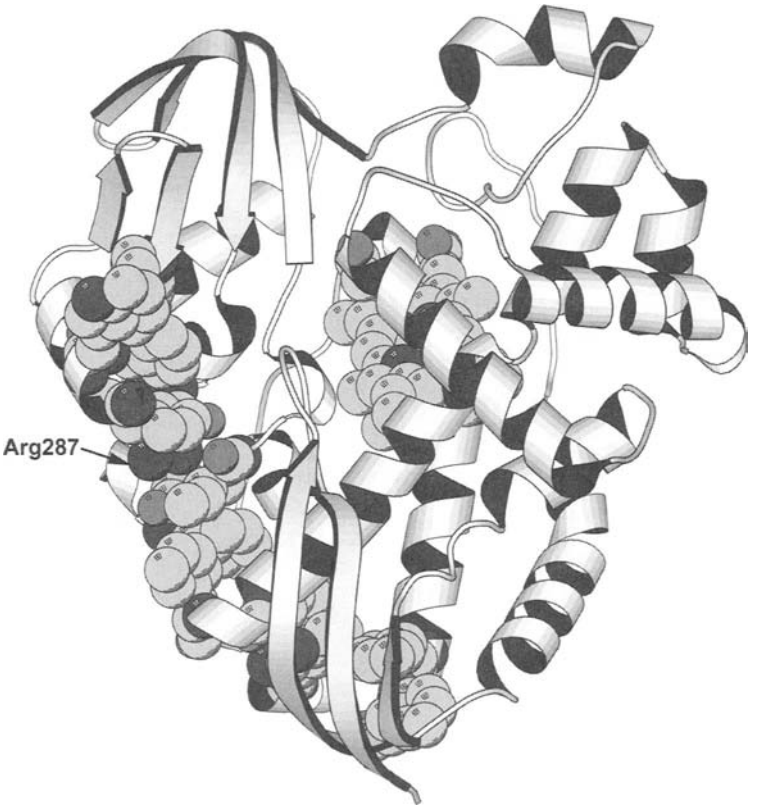

Figure 3.6. The structure of CYP119 showing the aromatic cluster that is thought to be responsible for thermal stability. The cluster also contains an Arg residue (Arg287) which is sandwiched between two tyrosine residues and hence, contributes to the π-stacking interactions of the aromatic cluster.

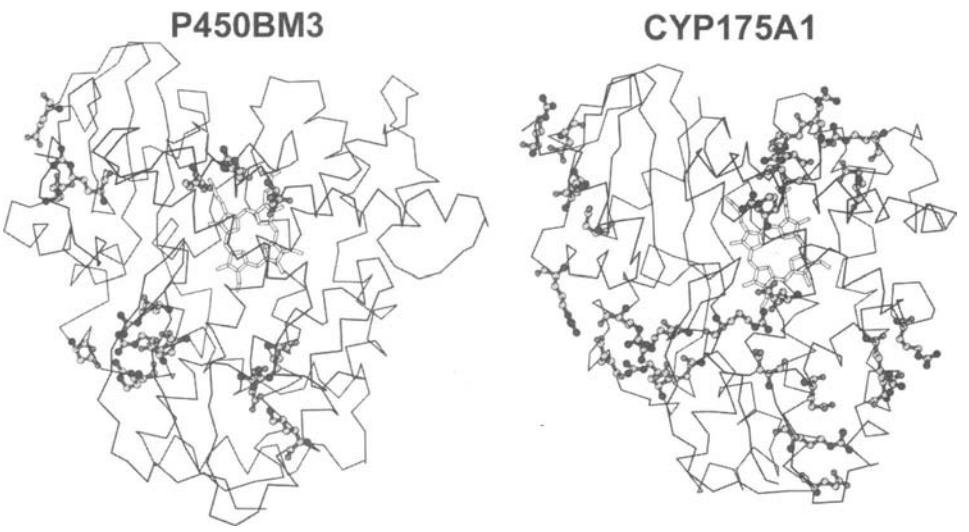

Figure 3.7. A comparison between P450BM3 and the thermal stable P450, CYP175A1, showing the salt bridge networks in both proteins.

aromatic cluster shows that the melting temperature can be lowered 10–15°C[24] further implicating aromatic clustering as a key factor in thermal stability.

The second thermophilic P450 to be discovered was CYP175A1 from *Thermus thermophilus*[25] which melts at 88°C. Like CYP119, CYP175A1 is also shorter than most other P450s and contains 378 residues. CYP175A1 most closely resembles P450BM3 but with shorter surface loops. CYP175A1 lacks the aromatic clustering observed in CYP119 and hence, the structural basis for thermal stability lies elsewhere. Yano *et al.*[25] carried out a detailed comparison of salt bridge networks in various P450s and found that CYP175A1 contains a larger fraction of salt bridges that contain three or more residues. As shown in Figure 3.7, CYP175A1 has 26 residues involved in 8 salt bridge networks while the closest homologue to CYP175A1, P450BM3, has 14 residues participating in 4 salt bridge networks.

4. Membrane P450s

In contrast to prokaryotic P450s, eukaryotic P450s are generally membrane-bound proteins. Most eukaryotic P450s are incorporated into the endoplasmic reticulum. However, several mammalian P450s that participate in the synthesis of sterols, steroids, and bile acids are located on the matrix side of the mitochondrial inner membrane. A longer N-terminal polypeptide chain of roughly 30–50 amino acids precedes the catalytic domain in eukaryotic P450s and mediates membrane targeting. In the case of mitochondrial P450s, the targeting sequences are cleaved during import of the protein into mitochondria[26]. In contrast, the leader sequence of microsomal P450s is retained and is co-translationally inserted into the endoplasmic reticulum[27]. The insertion process stops at the end of a hydrophobic stretch of roughly 20 amino acid residues, and the catalytic domain of microsomal P450s resides on the cytoplasmic side of the endoplasmic reticulum. A short region that generally contains positively charged residues links the catalytic domain to a conserved proline rich motif at the N-terminus of the structurally conserved P450 fold. The N-terminal transmembrane domain extends across the membrane and is unlikely to be closely associated with the catalytic domain (Figure 3.8). This N-terminal domain is not required for function as illustrated by the expression and successful reconstitution of several P450 monooxygenases in which this region was deleted[28–32].

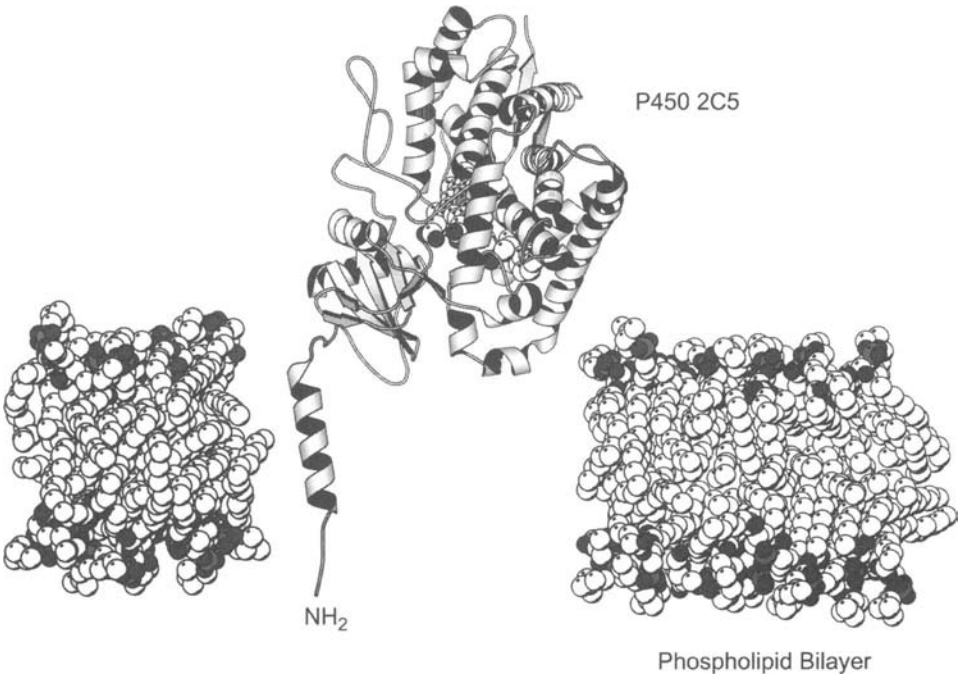

Figure 3.8. Hypothetical model for the membrane binding of microsomal P450s. The cartoon depicts the experimentally determined fold of the modified CYP2C5 catalytic domain, PDB: 1N6B, attached to a hypothetical model for the N-terminal transmembrane helix. The latter is flanked by a modeled array of phospholipid molecules depicted as CPK atoms. The heme and bound substrate, DMZ, of CYP2C5 are also rendered as CPK atoms.

Another major difference relative to prokaryotic P450s is the insertion of a longer polypeptide chain between helices F and G in eukaryotic P450s. This region exhibits two short helices, F′ and G′, in the structures of CYP2C5 (Figure 3.9) and CYP2B4, a single, longer F′ helix in P450 2C8, and a more relaxed coiled conformation in CYP2C9. This portion of the structure is in close juxtaposition to the region between the proline-rich motif at the N-terminus of the catalytic domain and helix A, and together they form a hydrophobic surface near the N-terminus of the protein[33]. Epitope mapping studies of the related enzyme CYP2B4[34] suggest that this portion of the structure is in close proximity to and possibly buried in the membrane as illustrated in Figure 3.8. Similar interactions may underlie the binding of mitochondrial P450s to the matrix surface of the inner membrane. As mitochondrial P450s lack the N-terminal transmembrane helices found in microsomal P450s, the catalytic domain must interact more extensively than their microsomal counterparts with the hydrophobic core of the lipid bilayer because detergents are required to release mitochondrial P450s from the membrane. In contrast, the catalytic domain of microsomal CYP2C5 is released by high salt buffers when it is expressed as a truncated construct that does not contain the N-terminal transmembrane helix[28, 29].

The model shown in Figure 3.8 is consistent with additional observations. Antibody epitope mapping studies indicate that extensive portions of the surfaces of drug metabolizing P450s are accessible to the antibodies, reviewed in ref. [35]. As shown in Figure 3.10, most of the epitopes reside along the edges of the protein with the exception of the tip of the protein near the N-terminus of the catalytic domain. The tilt of the heme relative to the membrane has been estimated for CYP17 and CYP21 based on the rate of decay of the absorption anisotropy following photodissociation of carbon monoxide complexes of each protein.

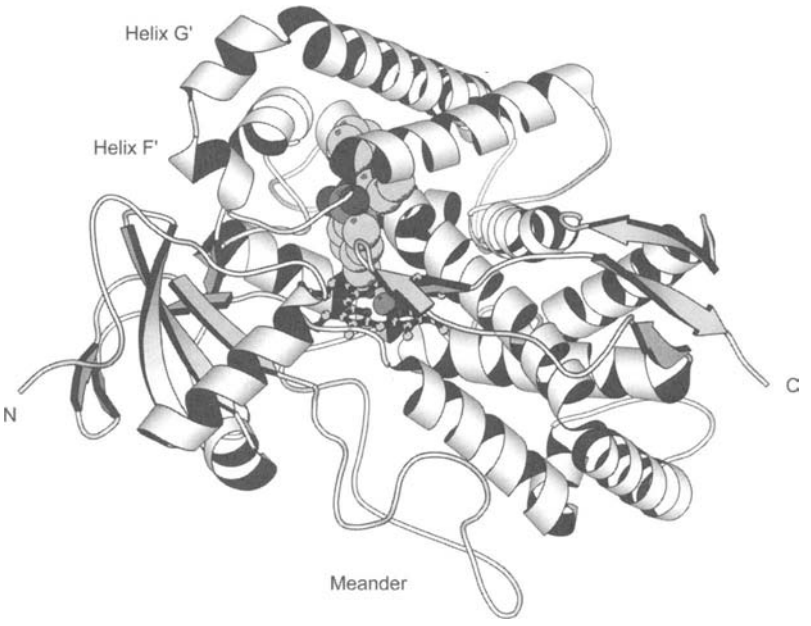

Figure 3.9. A side view showing the overall fold of modified CYP2C5. The largest insertions of additional polypeptide chain relative to prokaryotic P450s occur for the N-terminal region depicted in Figure 3.8, the meander region, and between helices F and G. The latter exhibits two short helical regions labeled F′ and G′.

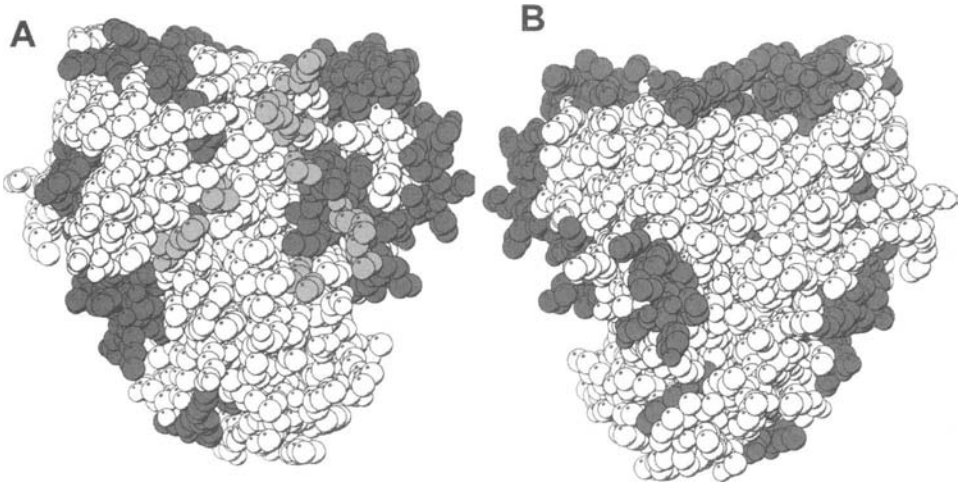

Figure 3.10. CPK rendering of the (A) proximal and (B) distal surfaces of modified CYP2C5. Antibody epitopes recognized when the protein is bound to microsomal membranes are dark gray, as reviewed in ref. [40]. Several conserved amino acid side chains that have been implicated in P450 reductase interactions with CYP2B4[40] are medium gray. The orientation of the protein is similar to that depicted in Figure 3.8 with the N-terminus of the catalytic domain positioned toward the bottom of the figure.

The results of these studies suggest that the angle for the orientation of the heme relative to the membrane surface is either 50° or 70° (See ref. [36]). The latter value is consistent with the orientation seen in Figure 3.8 and leads to significant solvent exposure for the surfaces of the catalytic domain. Atomic force microscopy experiments estimate that the height of P450 2B4 above a model phospholipid membrane is roughly 35–45 nm[37]. This would require a portion of the protein to be buried in the membrane, and this is likely to be the hydrophobic region near the N-terminus of the catalytic domain. Studies of the association of P450 2B4 with Langmuir–Blodget, phospholipid monolayers indicate that the protein displaces an area that is larger than a single transmembrane helix[38]. This result would be consistent with the penetration of the hydrophobic tip of the protein into the lipid layer. A lower angle of the heme plane would juxtapose a larger surface of the helix F–G region with the membrane surface, which is hydrated and largely formed by the zwitterionic phospholipid head groups. A steeper angle would bury the hydrophobic tip deeper into the membrane. The propensity of the helix F to helix G region to form helical structures rich in aromatic residues would enable this region to penetrate more deeply into the membrane because the hydrogen bonding in the helices would diminish the energetic cost of burying the peptide bonds in a hydrophobic environment[39].

Membrane interactions with the catalytic domain of microsomal P450s could promote the transfer of hydrophobic substrates from the membrane to the P450 and could also orient the protein to facilitate interactions with P450 reductase as the two proteins diffuse along the surface of the endoplasmic reticulum. Mutagenesis experiments[40] suggest that a group of relatively conserved, positively charged amino acids on the proximal surface of CYP2B4 interact with the reductase (Figure 3.10). Significant insertions of additional amino acid residues relative to most prokaryotic P450 structures are also present on the proximal surface of the protein, and these are also in the structure of P450BM3. The additional residues form the J′ helix extend a portion of the polypeptide chain termed the meander region that precedes the beta-turn containing the cysteine that provides the axial ligation for the heme. The corresponding region of CYP2C5 is illustrated in Figure 3.9. The functional importance of this insertion is unclear, but it resides in close proximity to the probable site of P450 reductase binding as discussed in the next section.

5. Electron Transfer Complexes

An important advance in understanding P450 monooxygenase electron transfer systems was the solution of the P450 reductase structure[41]. With the addition of the first mammalian P450 structure, CYP2C5, the way is now open for understanding how these two microsomal proteins interact and transfer electrons. Nevertheless, the *Bacillus megaterium* fatty acid monooxygenase system, P450BM3, has so far served as the best model system for understanding reductase–P450 interactions. Although P450BM3 is a bacterial enzyme, P450BM3 is more closely related in sequence, structure, activity, and redox partner to microsomal P450s than to other bacterial P450s. The unique feature of P450BM3 is that the diflavin P450 reductase is linked to the C-terminal end of the heme domain thus giving a catalytically self-sufficient enzyme.

A significant advance was made when Sevrioukova *et al.*[42] succeeded in crystallizing a P450BM3 construct that contains just the heme and FMN domains. The structure (Figure 3.11) shows that the FMN domain docks on the proximal surface of the P450, which was expected based on complementary electrostatic surfaces and mutagenesis studies. Nevertheless, the heme–FMN construct used to solve this structure was missing the FAD domain and the linker connecting the heme and FMN domains had been proteolyzed during crystallization, thus raising the possibility that the structure is an artifact of crystallization. In addition, the structure of the P450BM3 complex is not compatible with the P450 reductase structure. As shown schematically in Figure 3.12, the FMN and FAD in P450 reductase form a direct nonbonded contact. In order for the FMN domain to dock onto the proximal surface of P450, there must be a large structural change which enables the FAD and FMN domains to move apart (Figure 3.12). Indeed, there are good indications that the linker connecting the FAD and FMN domains is quite flexible. One of the more important studies related to the question of domain flexibility is the structure of

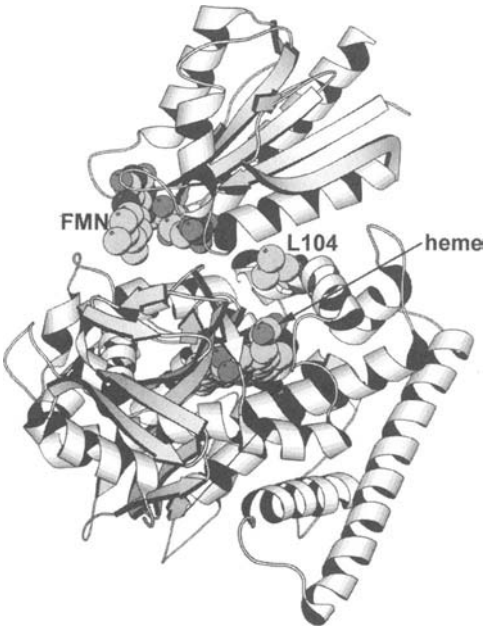

Figure 3.11. Structure of complex formed between the heme and FMN domains in P450BM3. The FMN domain docks into the concave depression on the heme domain proximal surface.

the homologous reductase domain in sulfite reductase. This enzyme resembles P450BM3 in having a heme domain attached to a FMN/FAD reductase domain. The FAD domain of sulfite reductase is very similar to the FAD domain of P450 reductase with an rms deviation of between 1.3 and 1.5 Å[43]. However, the FMN domain is not visible in electron density maps in four different crystal forms indicating that the FMN–FAD linker domain is quite flexible allowing the FMN domain to adopt multiple orientations relative to the FAD domain. As it must, the large void in the crystal lattice can accommodate the FMN module, but packing considerations show that the possible interactions between the FMN and FAD modules are quite different than in P450 reductase[43]. This raises the possibility that the P450 reductase structure may have captured the FMN domain in one possible orientation while the P450BM3 electron transfer complex captured the orientation of the FMN domain required for proper docking to P450.

The P450BM3 electron transfer complex structure also is consistent with mutagenesis and chemical modification studies. Sevrioukova *et al.*[44] changed key residues on the heme domain that lie at the interface between the heme and FMN domains. Replacing Leu104 of P450BM3 with a Cys (Figure 3.11) at the interface should not alter binding or electron transfer because replacing Leu with a smaller side chain should not cause any steric problems in forming the proper complex. However, covalent modification of the mutant Cys104 side chain with a large fluorophore should interfere with electron transfer. For these studies laser flash photolysis was used wherein a laser flash photoreduced a potent reductant, deazariboflavin, which in turn reduces the FMN in the complex. The reduced FMN semiquinone then reduces the P450 heme. As predicted, mutation of Leu104 to Cys had no effect, while chemical modification of Cys104 dramatically decreased the FMN-to-heme electron transfer rate, thus implicating Leu104 as an important residue in forming the proper electron transfer complex.

A second prediction from the P450BM3 electron transfer complex structure that can be tested is the electron transfer path. The heme-FMN domain interface is shown in Figure 3.13. A particularly noteworthy feature at the interface is the participation of water molecules. Waters form H-bonding bridges between the two domains while there are only two direct H-bonds between side chains. The closest point of contact between the two domains places the FMN about 4 Å from the peptide backbone of Gln387. The peptide chain from Gln387 to the heme ligand, Cys400, could constitute an electron transfer path. To test this hypothesis, Gln387 was converted to Cys and modified with (4-bromomethyl-4′-methylbipyridine)[bis(bipyridine)]ruthenium(II)[45]. The covalently attached Ru(II) is photoreduced, and the rate of reduction of the heme Fe(III) to Fe(II) by the photogenerated Ru(I) was followed. The same experiment was carried out with Ru(II) attached to Cys60. Both Cys60 and Cys387 are about the same distance from the heme but electron transfer from Cys60 to Ru(II) must make "through-space" jumps, while there is a continuous covalent connection between Cys386–Ru(II) and the heme ligand, Cys400. In the case of Cys387–Ru(II), the heme iron was reduced at a rate of $4.6 \times 10^5\ s^{-1}$, while Cys60–Ru(II) did not reduce the heme iron. These results indicate that if the crystal structure

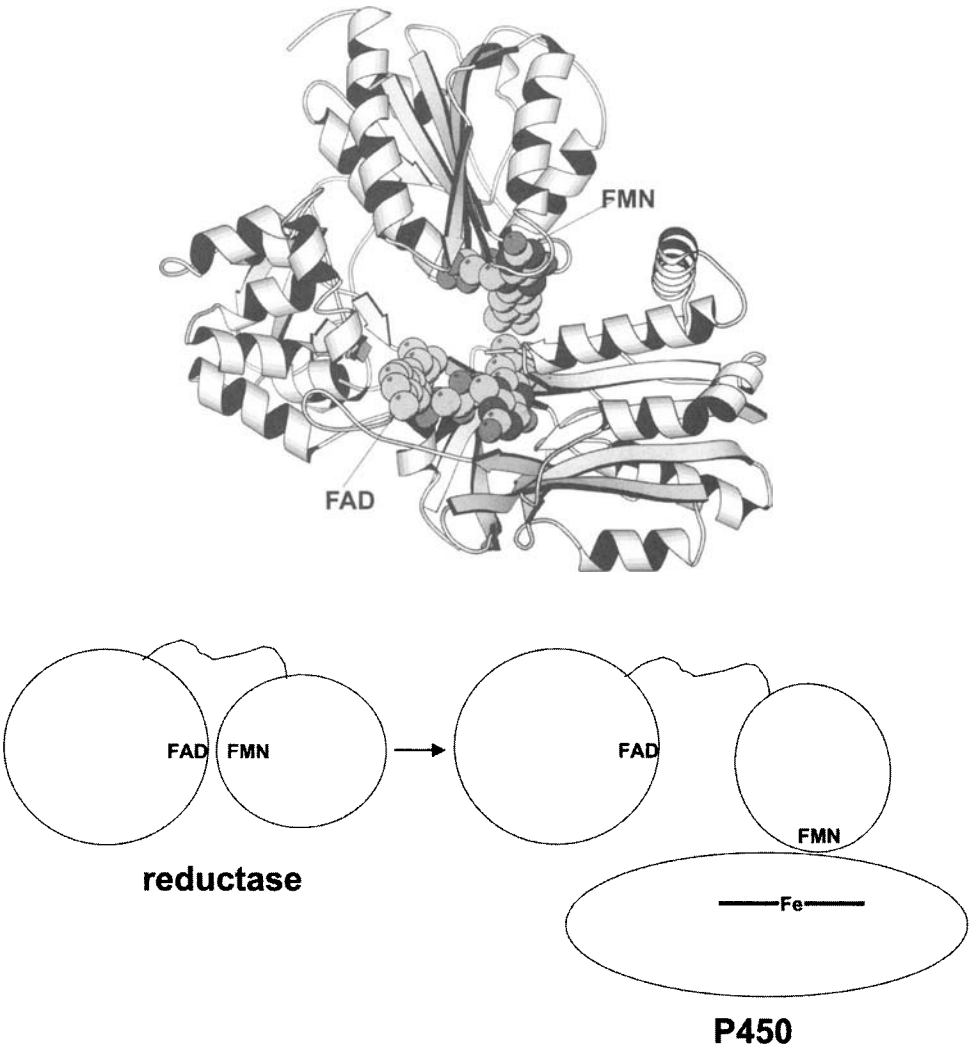

Figure 3.12. The crystal structure of P450 reductase[41]. Note that the FMN and FAD are in direct contact. The schematic diagram illustrates that it may be necessary for the FMN and FAD domains to separate to enable the FMN domain to dock onto the P450 prior to the FMN-to-heme electron transfer reaction.

of P450BM3 electron transfer complex is functionally relevant, then the electron transfer reaction can readily proceed along the direct point of contact between the FMN and heme domain.

Another recent advance in P450 electron transfer is the solution of both the putidaredoxin (Pdx)[46] and putidaredoxin reductase (Pdr)[47] crystal structures. Thus, the structure of all components of the P450cam monooxygenase system now are known. The Pdx and Pdr structures are shown in Figure 3.14 together with the crystal structure of the adrenodoxin–adrenodoxin reductase complex[48]. The Pdx and adrenodoxin (Adx)[49] structures clearly are very similar. However, Pdr and adrenodoxin reductase (Adr)[50] exhibit large differences. The FAD site is less exposed in Pdr owing to an additional β-pair situated near the cofactor. In addition, the C-terminal region of Pdr (Figure 3.14) is positioned very differently than in Adr. Note that this segment in Pdr blocks part of

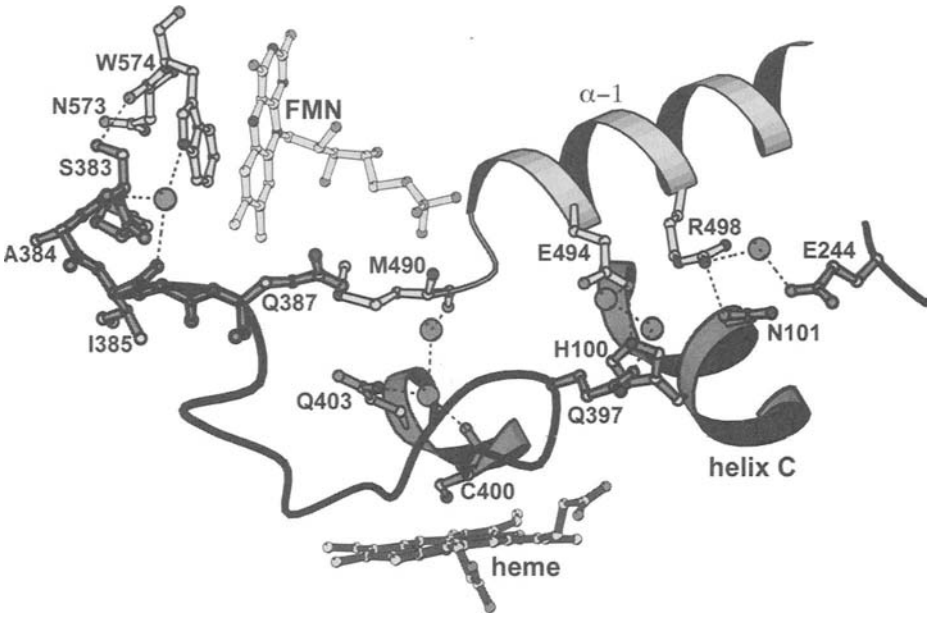

Figure 3.13. A close-up view of the interface formed between the heme and FMN domains in the P450BM3 electron transfer complex. The heme domain is more darkly shaded. There are only two direct H-bonds between the two domains: His100(heme)-Glu494(FMN) and Asn101(heme)-Arg498(FMN). The remainder of the electrostatic interactions are formed by bridging water molecules. Note that the FMN directly contacts the heme domain near Gln387. The section of polypeptide leading from Gln387 to the Cys400 ligand and heme could provide a selective electron transfer conduit.

the binding site for Adx in the Adx–Adr complex. Therefore, if Pdx and Pdr form a complex similar to the Adr–Adx complex, then the C-terminal domain in Pdr must move. This seems unlikely since the C-terminal region that would be required to move is composed of β-sheets that tie this region to the main body of the protein. Therefore, Pdx forms a complex with Pdr that must be quite different than the Adx–Adr complex. Also shown in Figure 3.14 is the glutathione reductase structure[51], which more closely resembles Pdr than does Adr. Note that both Pdr and glutathione reductase have the common domain similarly positioned which limits exposure of the FAD. This similarity is especially interesting since Pdr exhibits an NAD(H)-dependent dithiol/disulfide oxidoreductase activity similar to glutathione reductase activities[52]. Whether or not this unexpected Pdr activity is physiologically relevant remains to be seen.

Although the structures of the various electron transfer complexes in the P450cam system are not known, a good deal has been learned about the primary forces involved in forming the complexes. Isothermal titration calorimetry shows that the Pdr–Pdx complex is entropically driven suggesting that nonpolar interactions dominate[53]. In contrast, electrostatic forces dominate the Pdx–P450cam complex. These equilibrium thermodynamic studies agree with kinetic results obtained using laser flash photolysis methods to measure the P450–Pdx and Pdx–Pdr electron transfer rates[54].

Despite the lack of structural data on the complexes, Pochapsky *et al.* have developed a hypothetical model of the P450cam–Pdx complex using the crystal structure of P450cam and NMR structure of Pdx[55]. The Pochapsky model was developed well before the crystal structure of the P450BM3 complex was solved and was based on data derived from NMR, mutagenesis, and computational studies. Quite interestingly, both the P450cam–Pdx and P450BM3 complexes utilize the same proximal surface of P450 for the docking

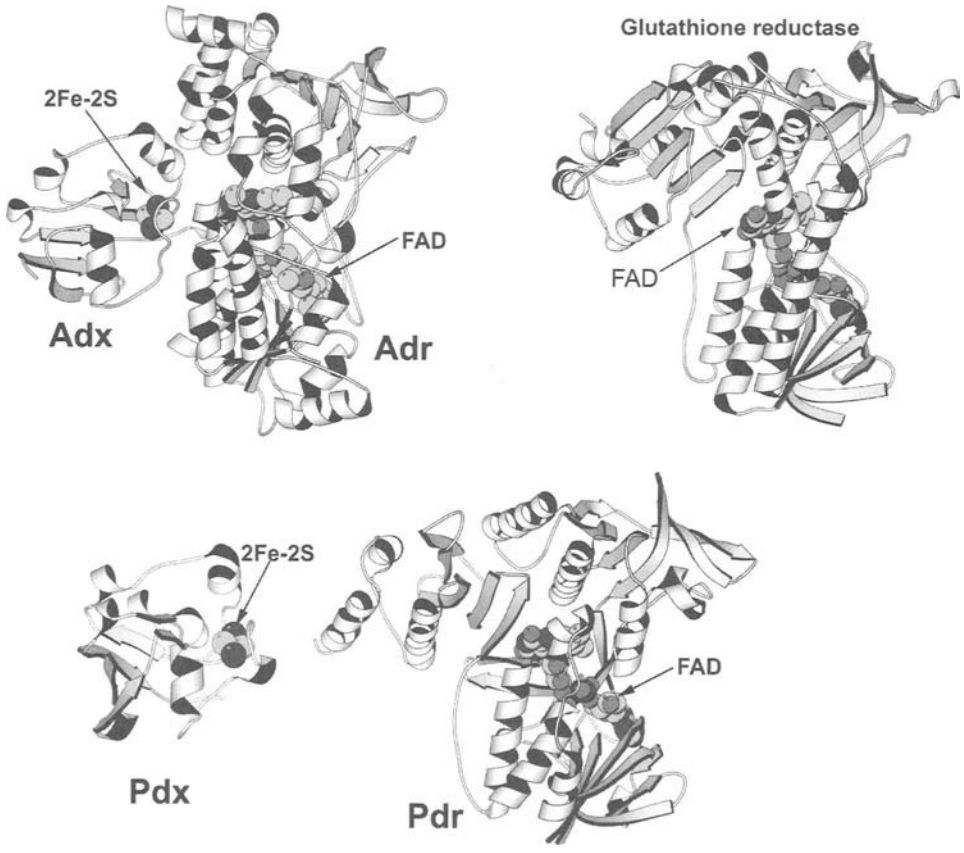

Figure 3.14. Structures of the adrenodoxin (Adx)–andrenodoxin reductase (Adr) complex, putidaredoxin (Pdx), and putidaredoxin reductase (Pdr). For comparisons, the structure of glutathione reductase also is shown.

of redox partners (Figures 3.11 and 3.15). This makes sense since the proximal region is the closest approach of heme to the surface and thus affords the closest approach of redox active cofactors.

6. Substrate Complexes

At present, the structure of five prokaryotic P450–substrate complexes are known (Figures 3.16 and 3.17). P450epoK, the newest member of this group[56], catalyzes the 12,13-epoxidation of epothilones (Figure 3.18) in *Streptomyces coelicolor*[57]. Like Taxol, epothilones block microtubule depolymerization thus arresting the cell cycle in the G2-M phase. As a result, epothilones show promise as anticancer agents. P450BSβ from *Bacillus subtilis* is a novel enzyme that has the P450 fold but catalyzes the peroxide-dependent hydroxylation of fatty acids[58]. As shown in Figure 3.17, an OH group is attached to the polar carboxyl end of the substrate which means the carboxyl head group must be positioned deep in the active site. P450BSβ has adapted to accommodate the carboxyl group by having an Arg residue on the I helix that electrostatically stabilizes the carboxyl head group (Figure 3.17). In the proposed peroxide activation mechanism, the fatty acid carboxyl group serves an acid–base catalytic function[58] similar to the distal histidine in peroxidases. P450BSβ provides a fascinating new example on the adaptability of P450s to the requirements of different metabolic pathways.

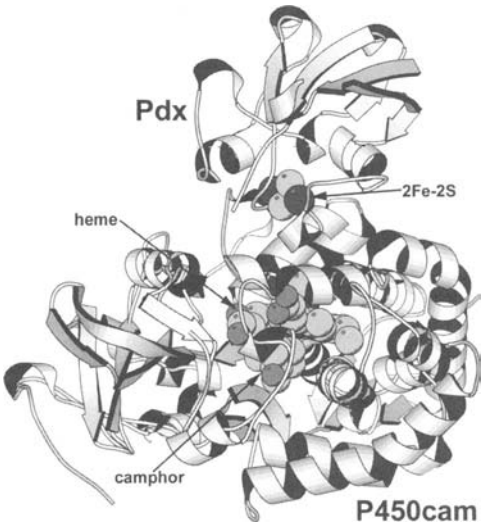

Figure 3.15. The P450cam–Pdx complex based on NMR and modeling studies[77]. Pdx docks onto the proximal surface of P450cam which is similar to the complex formed in P450BM3 (Figure 3.11).

The size and shape of the various substrates shown in Figure 3.16 are sufficiently diverse that the structural basis for what controls substrate specificity can, at least in part, be understood. As expected, all substrates are situated such that the atom to be hydroxylated is within 4–5 Å of the heme iron. Thus, regio- and stereo-selective hydroxylation by the hypothetical Fe(IV)-O species is achieved by specific protein–substrate interactions that hold the substrate in the correct position. The exception is P450BM3. The structure of the P450BM3 heme domain with palmitoleic acid[59] and N-pamitoylglycine[60] show that the fatty acid substrate is ≈7–8 Å from the iron which is too far for hydroxylation. However, NMR results indicate that the substrate moves to be within 3 Å of the iron upon reduction from Fe(III) to Fe(II)[61]. Precisely how reduction is linked to such a large repositioning of the substrate remains unknown.

P450cam and P450epoK represents the two extremes of substrate size and shape. Hence, a comparison between these two structures provides some insights on which regions of the structure change most in response to the requirements of substrate specificity. The two regions that differ the most between P450epoK and P450cam are the F, G, B' helices, and the F/G loop (Figure 3.19). The B′ helix is rotated 90° in P450epoK compared to P450cam. This reorientation opens the substrate-binding pocket thus making room for the thiazole ring of the substrate. The F and G helices do not superimpose well and the F/G loop adopts a substantially different conformation.

7. Conformational Adaptations to Substrates and Inhibitors

An unexpected insight into P450 dynamics came from the *S. solfataricus* CYP119 structure[22], the first known thermal stable P450[20]. The structure was solved in two crystal forms: one with imidazole and one with phenylimidazole coordinated to the heme iron. Compared to the phenylimidazole complex, in the imidazole complex, the C-terminal end of the F helix unwinds which increases the length of the F/G loop thus allowing the loop to dip down into the active and interact with imidazole ligand (Figure 3.20). In effect, the protein shapes itself around the ligand.

Conformational adaptations also contribute to the capacity of mammalian drug and xenobiotic metabolizing enzymes to recognize structurally diverse substrates. Rabbit microsomal CYP2C5, a drug and steroid metabolizing enzyme, has been co-crystallized with substrates of different sizes, flexibility, and polarity. Figure 3.21 depicts the binding of the anti-inflammatory drug diclofenac to CYP2C5 that catalyzes the 4′-hydroxylation of the dichlorophenyl ring of diclofenac. Diclofenac is positioned in CYP2C5 so that the flat surface of the dichlorophenyl ring faces the heme Fe[62]. The 4′-hydroxylation of diclofenac is likely to proceed through the formation of an epoxide intermediate formed by the addition of the iron oxo intermediate to the pi-electron system. The epoxide intermediate would rearrange to form the 4′-hydroxy product. The 3′ and 4′ carbons are 4.4 and 4.7 Å from the heme Fe, respectively[63].

Multiple sites of oxidation are frequently seen for substrates of drug metabolizing enzymes. This is likely to reflect either the capacity of the active site to bind the substrate in more than one orientation/location or motion of substrate within the active site cavity. The former case is evident for the structure of CYP2C5 complex with DMZ,

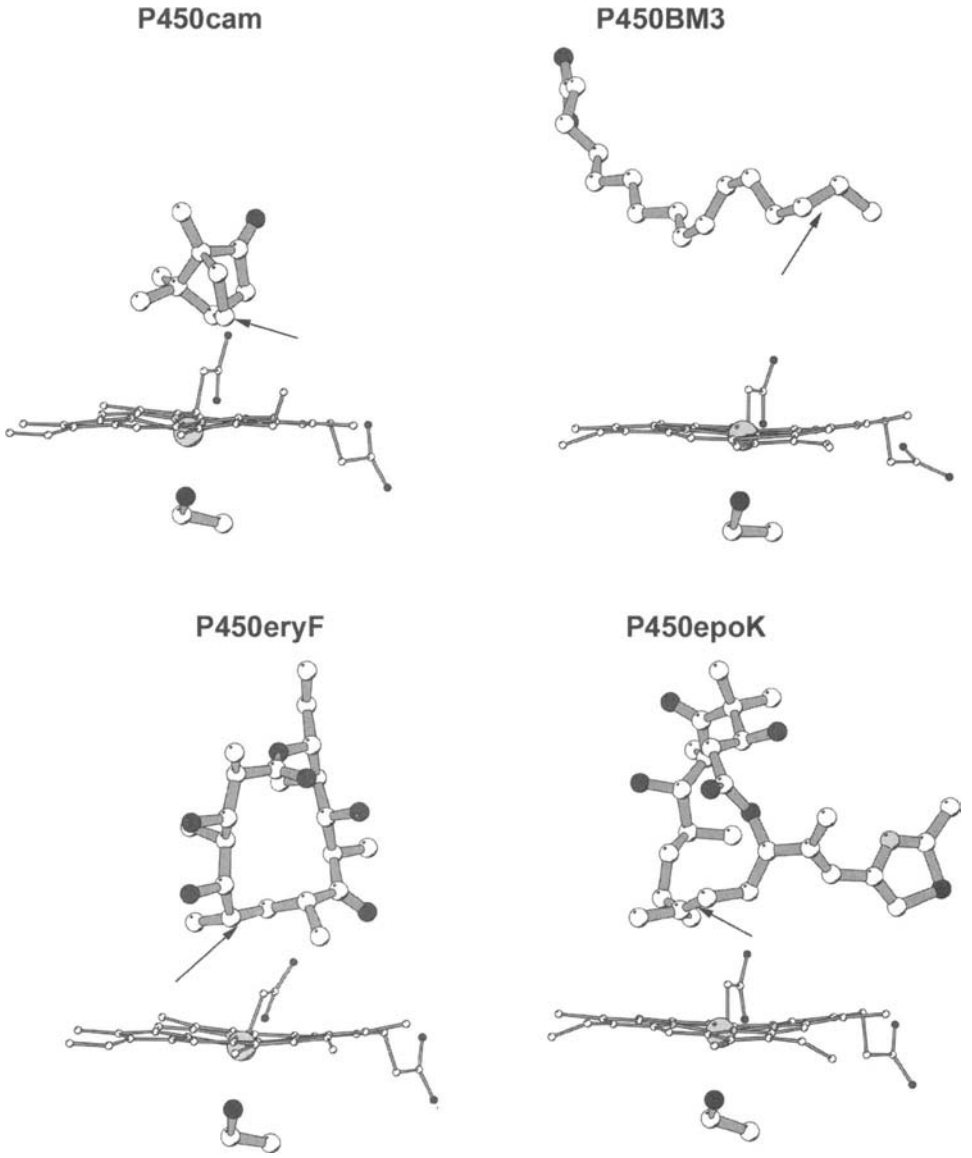

Figure 3.16. Active site structures of various P450–substrate complexes. The arrow indicates the carbon atom that is hydroxylated.

4-methyl-*N*-methyl-*N*-(2-phenyl-2*H*-pyrazol-3-yl)benzenesulfonamide (see ref. [63], Wester *et al.* 2003b). DMZ is a substrate for CYP2C5 as well as for each of the four human CYP2C enzymes[64]. Electron density maps and *in silico* docking studies indicate that the substrate binds in two alternate conformations, Figure 3.22. For DMZ, the primary site of hydroxylation (>98%) is the benzyllic methyl group. One conformation of DMZ places the benzylic methyl group 4.4 Å from the heme iron, and the reaction is likely to occur efficiently by a hydrogen abstraction mechanism. The second conformation places the other end of the molecule closest to the heme. However, DMZ is

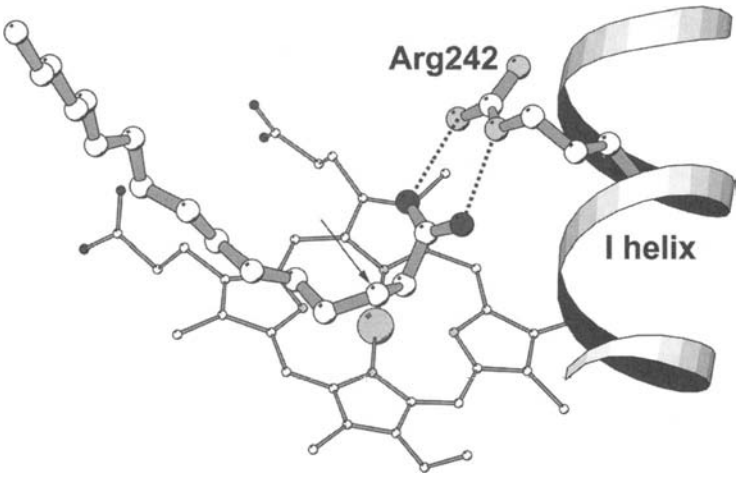

Figure 3.17. The substrate complex in P450BSβ[58]. This P450 utilizes peroxide to oxidize the atom indicated by the arrow. The I helix utilizes an arginine to help stabilize the carboxyl group of the substrate.

not located optimally for hydroxylation in this conformation as it is >5.9 Å from the heme iron, and the phenolic product accounts for <1% of the total products. The two conformations of DMZ overlap but occupy distinct portions of the active site cavity, which is larger than the substrate.

CYP2C5 exhibits adaptive changes when substrates bind. The largest, adaptive changes involve alterations in the conformations of the helix B–C region, in the locations of helices F and G, and the conformation of the region between the F and G helices. A comparison of the diclofenac and DMZ complexes illustrates differences that occur when bound substrates that are different in size, shape, and polarity (Figure 3.23). The change in the position of the F helix reflects differences in the space occupied by the two substrates near the heme Fe. Changes in the conformation of the B′ helix reflect adaptations that maximize interactions with each substrate and, in the case of diclofenac, that accommodate residual hydration in the distal portion of the active site that is not occupied by the substrate (Figure 3.23). These active site water molecules are ordered in a pattern that permits extensive intermolecular hydrogen bonding between water molecules, the protein and the substrate. This hydrogen bonding network is anchored by the polar carboxyl group of diclofenac and polar side chains in the distal portion of the active site. These interactions contribute to the affinity of the enzyme for diclofenac and the regioselective hydroxylation of the dichlorophenyl group. Human CYP2C9 exhibits similar regioselectivity for the oxidation of diclofenac and displays a high catalytic efficiency for the reaction. In contrast, the other human CYP2C enzymes generally exhibit a much lower catalytic efficiency and a more relaxed regioselectivity in that they hydroxylate both rings of the substrate.

8. Conformational Dynamics for Substrate Access

Substrate binding may involve rather large conformational changes. Once the P450cam structure became available, an immediate puzzle was how camphor gains access to the active site since the substrate is buried and there is no obvious opening. The substrate-free and -bound structures showed no differences although substrate-free P450cam exhibited much higher thermal motion in the B′, F, and G helices suggesting that the these regions must move to allow substrate to enter the active site[65]. That this region is quite flexible was demonstrated by binding of a ferrocene label to Cys85[66]. The positioning of the ferrocene into the active site results in unfolding of the B′ helix (Figure 3.24) and exposure of the active site. Although these changes may not mimic what happens when

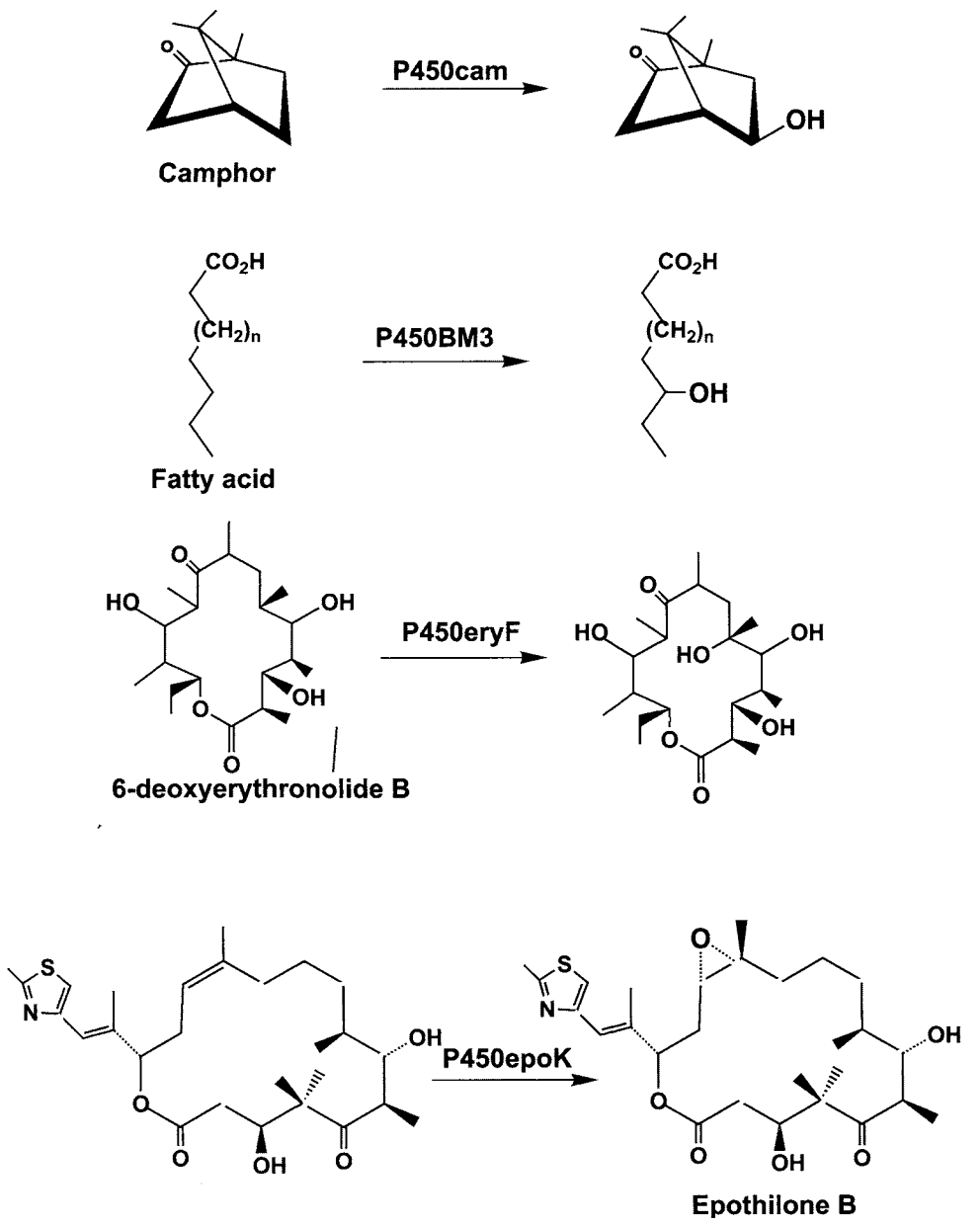

Figure 3.18. Reactions catalyzed by various P450s.

substrate binds and product leaves, this result does support the view that the B′ helix region can open to allow substrate to enter. Additional support for this view is provided by the structures of P450cam complexed with tether compounds. The tether compounds are designed to position a fluorescent reporter group at the enzyme surface by attaching it to a substrate analog that binds in the active site using a linker of the approximate length and size of the substrate access channel[67, 68]. As shown in Figure 3.25, the tether molecule occupies a continuous channel from the active site to the surface of

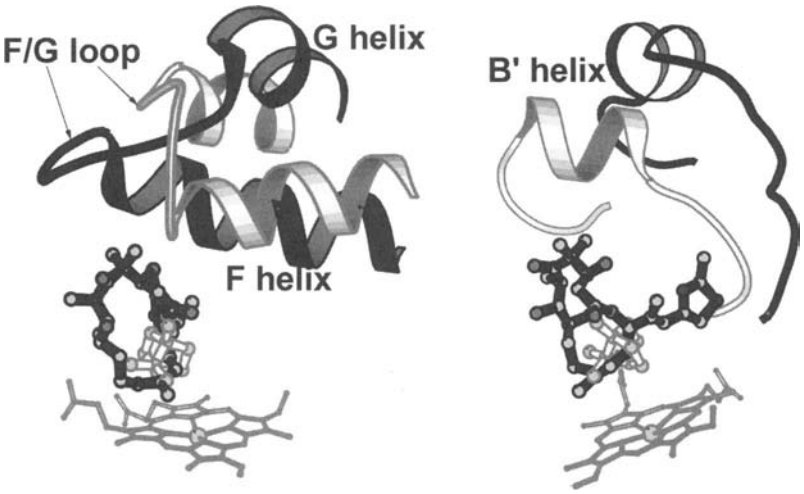

Figure 3.19. Differences between elements of structure that shape the substrate-binding pocket in P450cam (light shading) and P450epoK (dark shading). Note the differences in the position of the F/G loop and B′ helix.

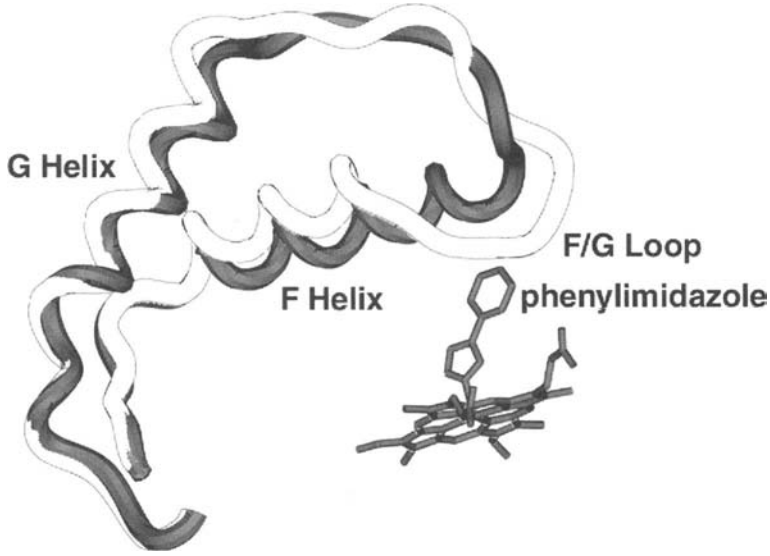

Figure 3.20. Ligand-induced conformational changes in CYP119. Compared to the phenylimidazole complex (dark shading), the C-terminal end of the F-helix in the imidazole complex unfolds which lengthens the F/G loop thus allowing the F/G loop to dip into the active site and interact with the iron-linked imidazole. Since phenylimidazole is larger than imidazole, the F/G loop cannot remain positioned in the active site complex. Therefore, the F/G helical region and loop "shapes" itself around the ligand bound in the active site.

P450cam that is created by displacement of helix B′ and the F–G loop.

The early work with P450cam, however, presented some experimental limitations. The initial diffraction quality crystals of P450cam had DTT bound in the active site. To obtain the substrate-free and -bound structures, DTT had to be back-soaked out or camphor soaked in. The relatively tight crystal lattice of P450cam very likely prevents the substrate-free structure from adopting

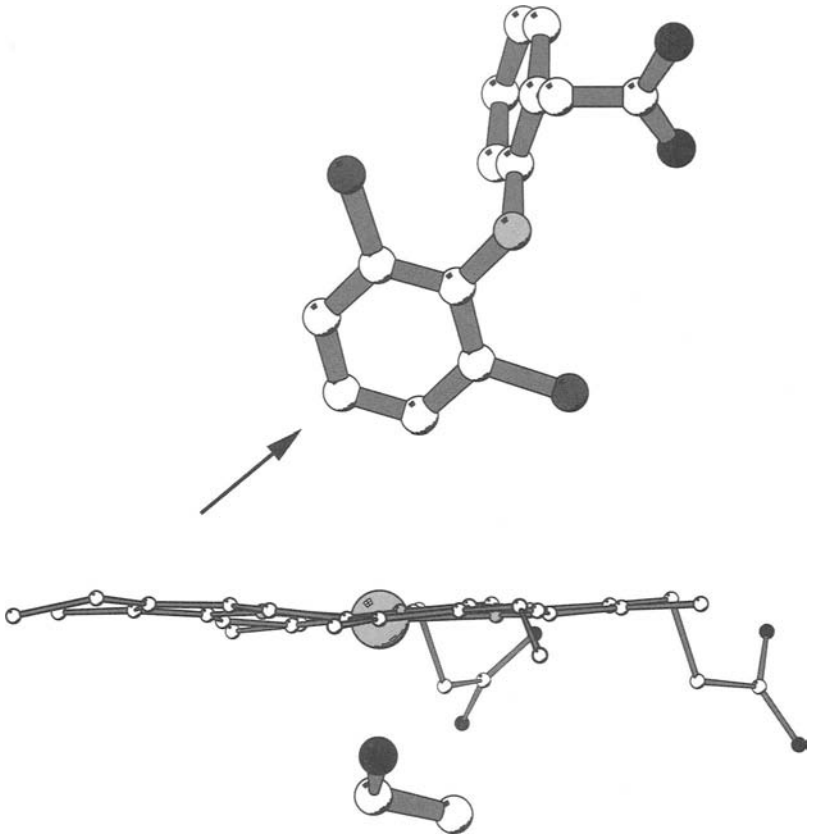

Figure 3.21. Diclofenac bound to CYP2C5, PDB: 1NR6. Hydroxylation of diclofenac at the 4′ carbon is likely to proceed through an intermediary epoxidation of the 3′–4′ carbon bond of the substrate. The 3′ and 4′ carbons are positioned at 4.4 and 4.7 Å, respectively, from the heme Fe. Polar interactions of the substrate carboxylate lead to a high degree of regioselectivity for oxidation of diclofenac by CYP2C5.

the open structure, although it remains unclear whether or not an open conformation is stable or is only a transient conformer.

The first clear indication that conformational changes are important in substrate binding was the structure of palmitoleic acid bound to P450BM3[59] which was followed by a higher resolution structure[60]. A solvent accessible surface diagram (Figure 3.26) illustrates how the substrate access channel is open in the substrate-free structure and closed in the substrate-bound structure. Quite interestingly, the experimentally observed conformational change was correctly predicted based on computational methods[69, 70] before the substrate-bound crystal structure was solved. The main motion involves the F and G helices sliding over the surface of the I helix. This motion closes off the entry channel indicating that substrates enter near the F/G loop region which is similar to P450cam.

Structures of several P450s exhibit open structures in the absence of substrates. P450nor is a novel, soluble eukaryotic P450 that reduces nitric oxide. The enzyme is directly reduced by NADH which binds directly to an open cleft between the F–G loop and the N-terminal β-sheet system of the enzyme[71]. Two recently determined structures for prokaryotic P450s that are thought to be involved in the oxidation of relatively large antibiotic compounds exhibit more open structures. One is OxyB[72], a P450 that is thought to be involved in the synthesis of vancomycin by *Amycolatopsis*

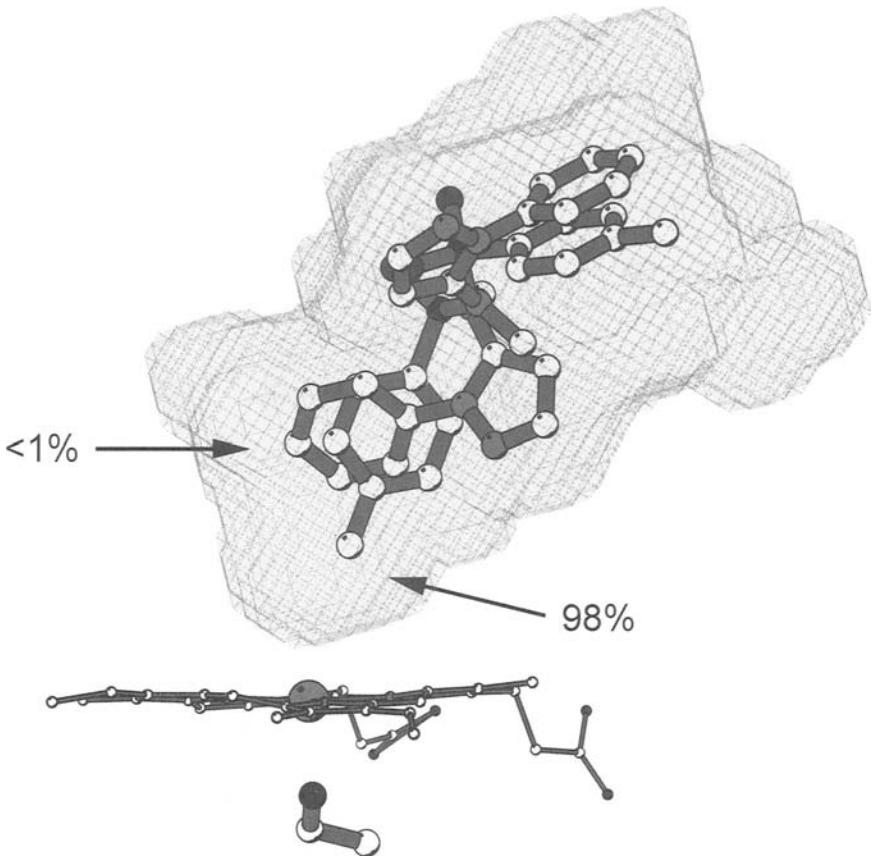

Figure 3.22. Binding of DMZ to CYP2C5, PDB: 1N6B. DMZ binds to the enzyme in two distinct locations depicted by the DMZ molecules with light and dark gray bonds. One orientation (light gray bonds) places the benzyllic methyl group of DMZ 4.4 Å from the heme iron, and oxidation of the benzyllic methyl group accounts for >98% of the observed products. The alternate orientation (dark gray bonds) places the phenyl ring at >6 Å from the heme Fe. Oxidation of the phenyl ring accounts for 1% of the products. A solvent accessible surface for the substrate-binding cavity is depicted by the light gray mesh.

orientalis. Helices F and G are rotated out of the active site in this structure. It is thought that the natural substrate of the enzyme is a relatively large, glycosylated heptapeptide. A similar positioning of helices F and G is also seen in the structure of CYP154C1 from *S. coelicolor A3(2)* (Figure 3.27) that oxidizes macrolide substrates[73]. In contrast to the structure seen for P450BM3, the region between helices B and C separates from the G helix to form a cleft that opens along helix I.

P450epoK presents a different picture. Here the substrate-free and -bound structures were separately crystallized[56], yet there is very little difference in structure. Substrate binding causes a slight tightening of the active site but there is no indication of the sorts of large motions observed with P450BM3. Caution must be exercised here because the energetics of adopting the open conformation must be balanced with the energetics of crystallization. With P450BM3, the open conformation was trapped due in part to crystal contacts. It may be that P450epoK simply prefers to crystallize in the "closed" form with or without substrate bound. The assumption here, of course, is that P450s must undergo open/close motions to allow substrate access even if we only observe the closed form in crystal structures.

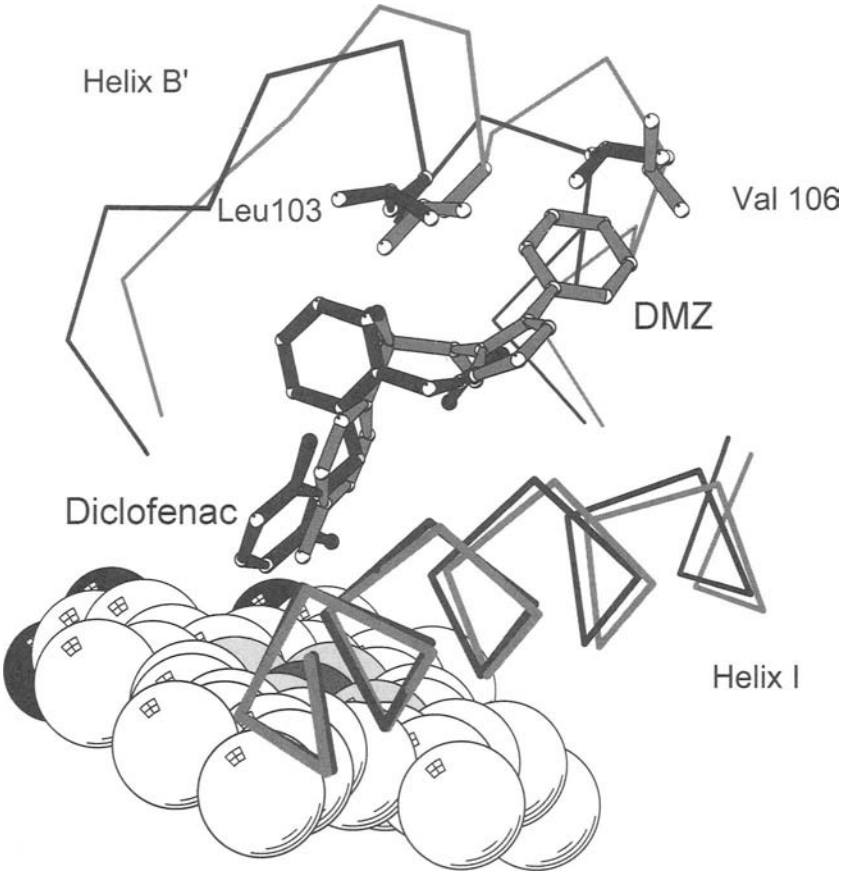

Figure 3.23. Conformational adaptations for substrate binding to CYP2C5. Among other changes, the position of helix B′ adapts to the presence of diclofenac and DMZ that differ in size and polarity. The DMZ complex is rendered in light gray, and the diclofenac complex is depicted in dark gray. Cα traces are shown for the helix B to C region and a portion of the helix I with the heme rendered as CPK atoms. The different positions of two active site side chains, Leu103 and Val106, are rendered as ball and stick figures, as are the two substrates.

While it would appear that the F/G loop region may provide the point of substrate entry and conformational dynamics for many P450s, the CYP51 structure[74] indicates that other access channels may be used. While CYP51 exhibits the normal P450 fold, there is an unprecedented break in the I helix (Figure 3.28). This break creates a new opening that runs roughly parallel to the heme as opposed to the F/G loop entry point which is perpendicular to the heme. Podust *et al.*[74] suggest that if the F/G loop region were to open, then the new opening must close. This offers the possibility that a concerted opening of one channel and closure of the other might provide a means for substrate to enter via one route but product depart via the other.

Eukaryotic P450s generally exhibit longer polypeptide chains between helices F and G than are seen in prokaryotic P450s, and this region interacts more extensively with the N-terminal β-sheet region, potentially limiting the opening of the protein in this direction. In addition, this region is likely to interact with the membrane. In contrast, the B′ helix region is not closely associated with the rest of the protein, suggesting that the flexibility of the helix B to helix C region is likely to shift

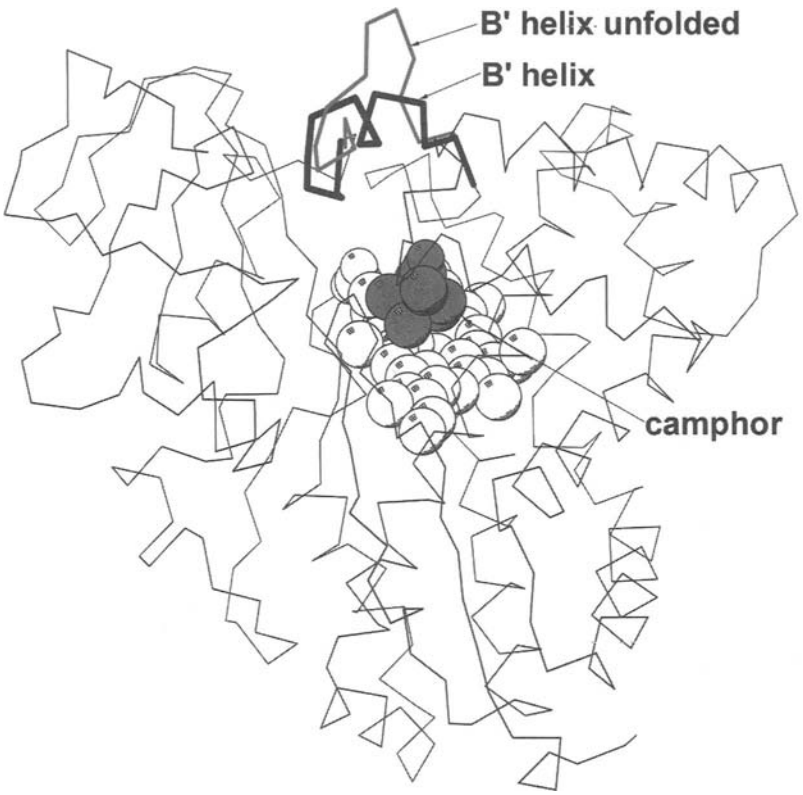

Figure 3.24. A comparison of the structures of B′ helix region in P450cam (dark shading) and the ferrocene attached to Cys85[66]. To accommodate the bulky ferrocene, the B′ helix must unfold (light shading) and move further away from the main body of the protein.

the opening to the active site to a direction along the helix I between the helix B′ to helix C loop and helix G. This is supported by the observation that progesterone can be soaked into CYP2C5 in crystals where the N-terminal β-sheet region and helices F and G are highly constrained by crystal packing. The solvent channel is closed by a single H-bonding interaction between K241 of helix G to the backbone carbonyl of V106 in helix B′ as well as a relatively weak van der Waals contact of V106 with H230 of helix G. Crystallization of CYP2B4 in an open conformation[75] supports this view; an open cleft is observed in this structure between the helix B′ to C loop, helix I and helix F to helix G regions.

A theoretical analysis of substrate-binding routes has helped to clarify the picture[76]. The computational approach predicts that the main substrate channel near the F/G loop is the same as that derived from the crystal structure but also predicts other possible routes of entry in P450cam, P450BM3, and P450eryF. In addition, novel routes of ligand exit were found. These pathways may be favored in other P450s that exhibit different packing interactions between the flexible components of the distal surface of the enzyme. These studies have also provided insights into the energetically accessible motions available to the various P450s.

Overall, the current picture is that while the P450 fold is conservative, it is quite flexible and can undergo rather large changes in response to the requirements of substrate specificity. The F/G helical region and B′ helix are subject to the greatest structural variation as well as flexibility. This is understandable considering the importance the

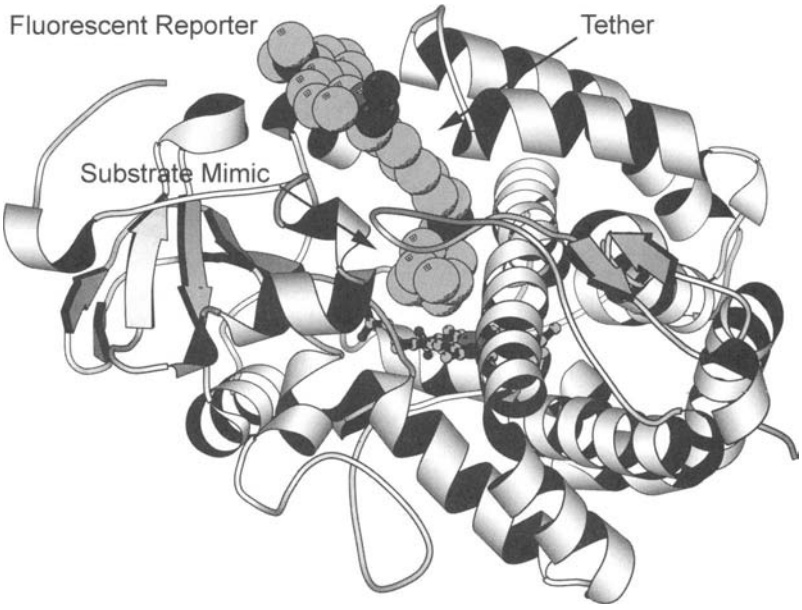

Figure 3.25. The structure of P450cam complexed with a tether compound adamantane-1-carboxylic acid-5-dimethylaminonaphthalene-1-sulfonylamino-octyl-amide rendered as CPK atoms, PDB: 1LWL. The heme is rendered as a ball and stick figure. The tether compound occupies an open channel between helices F and G, helix B′ and the β-sheet domain with the fluorescein moiety residing on the surface and the adamantane moiety positioned in the substrate-binding site.

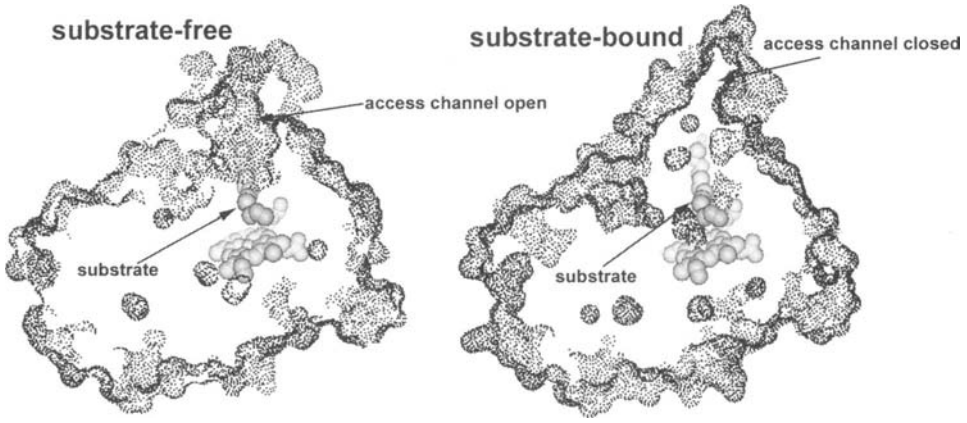

Figure 3.26. Solvent accessible surface diagrams of P450BM3 in the substrate-free and -bound forms.

F/G region and the B′ helix play in substrate entry and binding. Toward the goal of understanding selectivity, homology modeling has become an increasingly popular tool in P450 research. There are simply too many interesting P450s to expect the various crystal structures to be solved in a timely fashion. However, the structures we have in hand show quite clearly that homology modeling has a major challenge because the most difficult regions to predict are precisely those regions that are functionally most important. In many cases, the low degree of amino acid identity renders threading of these sequences onto experimentally determined structures ambiguous. This problem

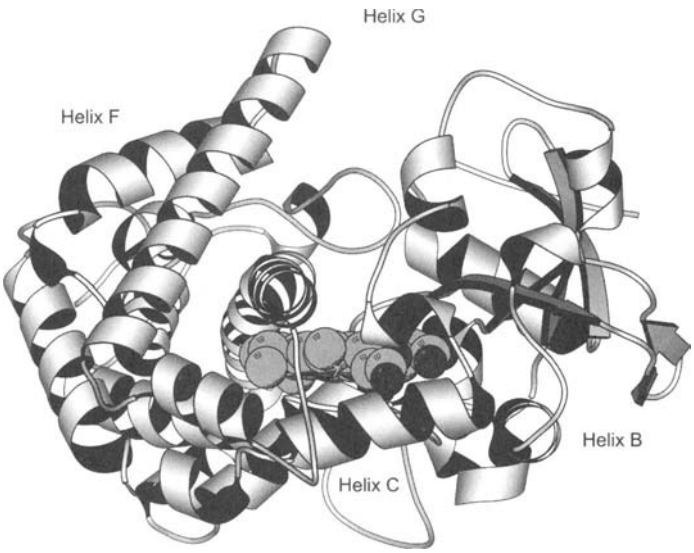

Figure 3.27. The structure of CYP154C1, PDB: 1GWI. A view along the N-terminal end of helix I is shown depicting the rotation of helices F and G up and away from the substrate-binding cavity. An open cleft runs through the molecule above the heme. The helix B to C segment resides on the opposite of the cleft in association with the β-sheet 1. The heme is rendered as CPK atoms.

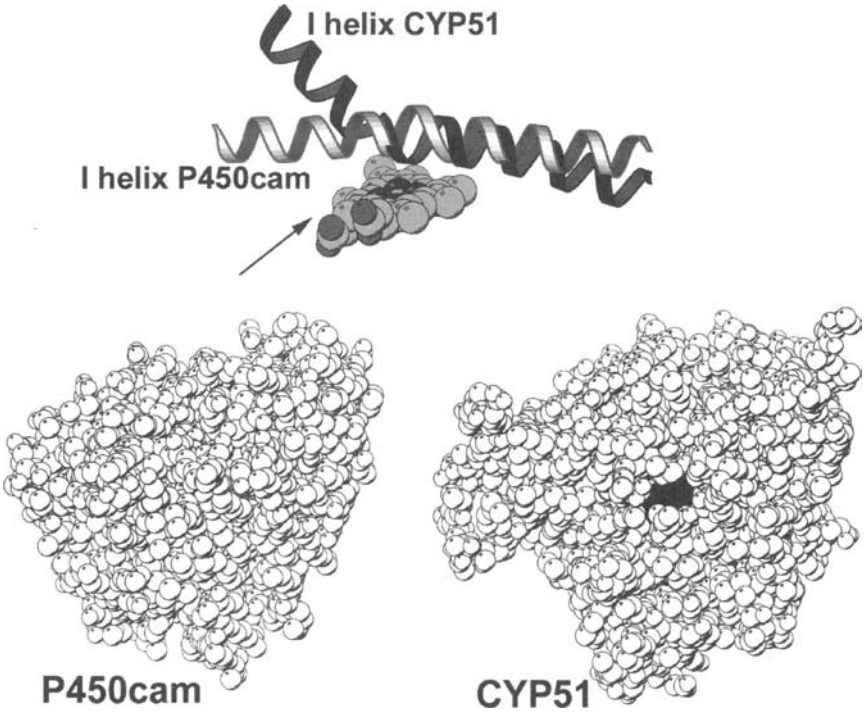

Figure 3.28. The top diagram shows the I helix in CYP51 (dark shading) and P450cam (light shading). The CPK diagrams are viewed along the plane of the heme and illustrate how the break in the I helix leaves the heme pocket open in CYP51.

has been largely overcome for the relatively large number of drug metabolizing enzymes in family 2 because alignments with known structures such as those of CYP2C and CYP2B families are relatively straightforward. However, the experimentally determined structures of the family 2 enzymes exhibit significant differences in the conformations of the flexible portions of the catalytic sites that underlie their functional diversity. Thus, a critical need to determine structures of specific drug metabolizing enzymes remains in order to accurately model substrate enzyme interactions.

Acknowledgments

TLP would like to thank members of the UCI P450 group, Huiying Li, Shingo Nagano, and Irina Sevrioukova, and NIH grant GM33688. EFJ would like to thank his colleagues at TSRI, Guillaume Schoch, Mike Wester, Jason Yano, and C. David Stout, as well as NIH Grant GM31001.

References

1. Poulos, T.L., B.C. Finzel, and A.J. Howard (1987). High-resolution crystal structure of cytochrome P450cam. *J. Mol. Biol.* **195**, 687–700.
2. Ravichandran, K.G., S.S. Boddupalli, C.A. Hasermann, J.A. Peterson, and J. Deisenhofer (1993). Crystal structure of hemoprotein domain of P450BM-3, a prototype for microsomal P450's. *Science* **261**, 731–736.
3. Sundaramoorthy, M., J. Terner, and T.L. Poulos (1995). The crystal structure of chloroperoxidase: A heme peroxidase–cytochrome P450 functional hybrid. *Structure* **3**, 1367–1377.
4. Crane, B.R., A.S. Arvai, D.K. Ghosh, C. Wu, E.D. Getzoff, D.J. Stuehr *et al.* (1998). Structure of nitric oxide synthase oxygenase dimer with pterin and substrate. *Science* **279**, 2121–2126.
5. Fischmann, T.O., A. Hruza, X.D. Niu, J.D. Fossetta, C.A. Lunn, E. Dolphin *et al.* (1999). Structural characterization of nitric oxide synthase isoforms reveals striking active-site conservation. *Nat. Struct. Biol.* **6**, 233–242.
6. Raman, C.S., H. Li, P. Martasek, V. Kral, B.S. Masters, and T.L. Poulos (1998). Crystal structure of constitutive endothelial nitric oxide synthase: A paradigm for pterin function involving a novel metal center. *Cell* **95**, 939–950.
7. Adman, E., K.D. Watenpaugh, and L.H. Jensen (1975). NH–S hydrogen bonds in *Peptococcus aerogenes* ferredoxin, *Clostridium pasteurianum* rubredoxin, and *Chromatium* high potential iron protein. *Proc. Natl. Acad. Sci. USA* **72**, 4854–4858.
8. Ueyama, N., T. Terakawa, M. Nakata, and A. Nakamura (1983). Positive shift of redox potential of $[Fe^2S_4(Z\text{-cys-Gly-Ala-OMe})_4]^{2-}$ in dichloromethane. *J. Am. Chem. Soc.* **105**, 7098–7102.
9. Ueyama, N., N. Nishikawa, Y. Yamada, T. Okamura, and A. Nakamura (1996). Cytochrome P-450 model (porphinato)(thiolatio)iron(III) complexes with and double NH-S hydrogen bonds. *J. Am. Chem. Soc.* **118**, 1286–1287.
10. Poulos, T.L. and B.C. Finzel (1984). Heme enzyme structure and function. In M.T. Mearn (ed.), *Peptide and Protein Reviews*, Vol. 4. Marcel Dekker, New York, pp. 115–171.
11. Chang, C.K. and T.G. Traylor (1973). Proximal base influence on the binding of oxygen and carbon monoxide to heme. *J. Am. Chem. Soc.* **95**, 8477–8479.
12. Doef, M.M., D.A. Sweigart, and P. O'Brien (1983). Hydrogen bonding from coordinated imidazole in ferric porphyrin complexes. Effect on the Fe(III)/Fe(II) reduction potential. *Inorg. Chem.* **22**, 851–852.
13. Nappa, M., J.S. Valentine, and P.A. Snyder (1977). Imidazolate complexes of ferric porphyrins. *J. Am. Chem. Soc.* **99**, 5799–5800.
14. Valentine, J.S., R.P. Sheridan, L.C. Allen, and P.C. Kahn (1979). Coupling between oxidation state and hydrogen bond conformation in heme proteins. *Proc. Nat. Acad. Sci. USA* **76**, 1009–1013.
15. Banci, L., I.I. Bertin, E.A. Pease, M. Tien, and P. Turano (1992). ^{1}H NMR investigation of manganese peroxidase from *Phanerochaete chrysosporium*. A comparison with other peroxidases. *Biochemistry* **31**, 10009–10017.
16. Vidakovic, M., S.G. Sligar, H. Li, and T.L. Poulos (1998). Understanding the role of the essential Asp251 in cytochrome p450cam using site-directed mutagenesis, crystallography, and kinetic solvent isotope effect. *Biochemistry* **37**, 9211–9219.
17. Benson, D.E., K.S. Suslick, and S.G. Sligar (1997). Reduced oxy intermediate observed in D251N cytochrome P450cam. *Biochemistry* **36**, 5104–5107.
18. Schlichting, I., J. Berendzen, K. Chu, A.M. Stock, S.A. Maves, D.E. Benson *et al.* (2000). The catalytic pathway of cytochrome p450cam at atomic resolution. *Science* **287**, 1615–1622.
19. Cupp-Vickery, J.R., O. Han, C.R. Hutchinson, and T.L. Poulos (1996). Substrate-assisted cataly-sis in cytochrome P450eryF. *Nat. Struc. Biol.* **3**, 632–637.

20. Wright, R.L., K. Harris, B. Solow, R.H. White, and P.J. Kennelly (1996). Cloning of a potential cytochrome P450 from the archaeon *Sulfolobus solfataricus*. *FEBS Lett.* **384**, 235–239.
21. McLean, M.A., S.A. Maves, K.E. Weiss, S. Krepich, and S.G. Sligar (1998). Characterization of a cytochrome P450 from the acidothermophilic archaea *Sulfolobus solfataricus*. *Biochem. Biophys. Res. Comm.* **252**, 166–172.
22. Yano, J.K., L.S. Koo, D.J. Schuller, H. Li, P.R. Ortiz de Montellano, and T.L. Poulos (2000). Crystal structure of a thermophilic cytochrome P450 from the archaeon *Sulfolobus solfataricus*. *J. Biol. Chem.* **275**, 31086–31092.
23. Park, S.Y., K. Yamane, S. Adachi, Y. Shiro, S.A. Maves, K.E. Weiss *et al.* (2002). Thermophilic Cytochrome P450 (CYP119) from *Sulfolobus solfataricus*: High resolution structural origin of its thermostability and functional properties. *J. Inorg. Biochem.* **91**, 491–501.
24. Puchkaev, A.V., L.S. Koo, and P.R. Ortiz de Montellano (2003). Aromatic stacking as a determinant of the thermal stability of CYP119 from *Sulfolobus solfataricus*. *Arch. Biochem. Biophys.* **409**, 52–58.
25. Yano, J.K., F. Blasco, H. Li, R.D. Schmid, A. Henne, and T.L. Poulos (2003). Preliminary characterization and crystal structure of a thermostable cytochrome P450 from *Thermus thermophilus*. *J. Biol. Chem.* **278**, 608–616.
26. Omura, T. and A. Ito (1991). Biosynthesis and intracellular sorting of mitochondrial forms of cytochrome P450. *Meth. Enzymol.* **206**, 75–81.
27. Sakaguchi, M. and T. Omura (1993). Topology and biogenesis of microsomal cytochrome P-450s. In K. Ruckpaul and H. Rein (eds.), *Medicinal Implications in Cytochrome P-450 Catalyzed Biotransformations*. Akademie Verlag, Berlin.
28. Von Wachenfeldt, C., T.H. Richardson, J. Cosme, and E.F. Johnson (1997). Microsomal P450 2C3 is expressed as a soluble dimer in *Escherichia coli* following modifications of its N-terminus. *Arch. Biochem. Biophys.* **339**, 107–114.
29. Cosme, J. and E.F. Johnson (2000). Engineering microsomal cytochrome P450 2C5 to be a soluble, monomeric enzyme. Mutations that alter aggregation, phospholipid dependence of catalysis, and membrane binding. *J. Biol. Chem.* **28**, 2545–2553.
30. Li, Y.C. and J.Y.L. Chiang (1991). The expression of a catalytically active cholesterol 7alpha-hydroxylase cytochrome P450 in *Escherichia coli*. *J. Biol. Chem.* **266**, 19186–19191.
31. Sagara, Y., H.J. Barnes, and M.R. Waterman (1993). Expression in *Escherichia coli* of functional cytochrome P450c17 lacking its hydrophobic amino-terminal signal anchor. *Arch. Biochem. Biophys.* **304**, 272–278.
32. Pernecky, S.J., J.R. Larson, R.M. Philpot, and M.J. Coon (1993). Expression of truncated forms of liver microsomal P450 cytochromes 2B4 and 2E1 in *Escherichia coli*: Influence of NH2-terminal region on localization in cytosol and membranes. *Proc. Natl. Acad. Sci. USA* **90**, 2651–2655.
33. Williams, P.A., J. Cosme, V. Sridhar, E.F. Johnson, and D.E. McRee (2000). The crystallographic structure of a mammalian microsomal cytochrome P450 monooxygenase: Structural adaptations for membrane binding and functional diversity. *Mol. Cell* **5**, 121–132.
34. De Lemos-Chiarandini, C., A.B. Frey, D.D. Sabatini, and G. Kreibich (1987). Determination of the membrane topology of the phenobarbital-inducible rat liver cytochrome P-450 isoenzyme PB-4 using site-specific antibodies. *J. Cell Biol.* **104**, 209–219.
35. Von Wachenfeldt, C. and E.F. Johnson (1995). Structures of eukaryotic cytochrome P450 enzymes. In P.R. Ortiz de Montellano (ed.), *Cytochrome P450: Structure, Mechanism, and Biochemistry*. Plenum Press, New York.
36. Ohta, Y., S. Kawato, H. Tagashira, S. Takemori, and S. Kominami (1992). Dynamic structures of adrenocortical cytochrome P-450 in proteoliposomes and microsomes: Protein rotation study. *Biochemistry* **31**, 12680–12687.
37. Bayburt, T.H. and S.G. Sligar (2002). Single-molecule height measurements on microsomal cytochrome P450 in nanometer-scale phospholipid bilayer disks. *Proc. Natl. Acad. Sci. USA* **99**, 6725–6730.
38. Shank-Retzlaff, M.L., G.M. Raner, M.J. Coon, and S.G. Sligar (1998). Membrane topology of cytochrome P450 2B4 in langmuir-blodgett monolayers. *Arch. Biochem. Biophys.* **359**, 82–88.
39. White, S.H., A.S. Ladokhin, S. Jayasinghe, and K. Hristova (2001). How membranes shape protein structure. *J. Biol. Chem.* **276**, 32395–32398.
40. Bridges, A., L. Gruenke, Y.T. Chang, I.A. Vakser, G. Loew, and L. Waskell (1998). Identification of the binding site on cytochrome P450 2B4 for cytochrome b5 and cytochrome P450 reductase. *J. Biol. Chem.* **273**, 17036–17049.
41. Wang, M., D.L. Roberts, R. Paschke, T.M. Shea, B.S. Masters, and J.J. Kim (1997). Three-dimensional structure of NADPH-cytochrome P450 reductase: Prototype for FMN- and FAD-containing enzymes. *Proc. Natl. Acad. Sci. USA* **94**, 8411–8416.
42. Sevrioukova, I.F., H. Li, H. Zhang, J.A. Peterson, and T.L. Poulos (1999). Structure of a cytochrome P450-redox partner electron-transfer complex. *Proc. Natl. Acad. Sci. USA* **96**, 1863–1868.
43. Gruez, A., D. Pignol, M. Zeghouf, J. Coves, M. Fontecave, J.-L. Ferrer *et al.* (2000). Four crystal

structures of the 60kDa falvoprotein monomer of the sulfite reductase indicate a disordered flavodoxin-like module. *J. Mol. Biol.* **299**, 199–212.

44. Sevrioukova, I.F., J.T. Hazzard, G. Tollin, and T.L. Poulos (1999). The FMN to heme electron transfer in cytochrome P450BM-3. Effect of chemical modification of cysteines engineered at the FMN-heme domain interaction site. *J. Biol. Chem.* **274**, 36097–36106.
45. Sevrioukova, I.F., C.E. Immoos, T.L. Poulos, and P. Farmer (2000). Electron transfer in the ruthenated heme domain of cytochrome P450BM-3. *Isr. J. Chem.* **40**, 47–53.
46. Sevrioukova, I.F., C. Gracia, H. Li, B. Bhaskar, T.L. Poulos (2003). Crystal structure of putidaredoxin, the [2Fe–2S] component of the P450cam monooxygenase system from Pseudomonas putida. *J. Molec. Biol.* **333**, 377–392.
47. Sevrioukova, I.F., H. Li, T.L. Poulos (2004). Crystal structure of putidaredoxin reductase from pseudomonas putida, the final structural component of the P450cam monooxygenase system. *J. Mol. Biol.* **236**, 889–902.
48. Muller, J.J., A. Lapko, G. Bourenkov, K. Ruckpaul, and U. Heinemann (2000). Adrenodoxin reductase-adrenodoxin complex structure suggests electron transfer path in steroid biosynthesis. *J. Biol. Chem.* **276**, 2786–2789.
49. Müller, A., J.J. Müller, Y.A. Muller, H. Uhlmann, R. Bernhardt, and U. Heinemann (1998). New aspects of electron transfer revealed by the crystal structure of a truncated bovine adrenodoxin, Adx(4-108). *Structure* **6**, 269–280.
50. Ziegler, G.A. and G.E. Schulz (2000). Crystal structures of adrenodoxin reductase in complex with NADP(+) and NADPH suggesting a mechanism for the electron transfer of an enzyme family. *Biochemistry* **39**, 10986–10995.
51. Mittl, P.R.E. and G.E. Schulz (1994). The structure of glutathione reductase from *Escherichia coli* at 1.86Å resolution: Comparison with the enzyme from human erythrocytes. *Protein Sci.* **3**, 799–809.
52. Sevrioukova, I.F. and T.L. Poulos (2002). Putidaredoxin reductase, a new function for an old protein. *J. Biol. Chem.* **277**, 25831–25839.
53. Aoki, M., K. Ishimori, and I. Morishima (1998). Roles of negatively charged surface residues of putidaredoxin in interactions with redox partners in P450cam monooxygenase system. *Biochim. Biophys. Acta* **1386**, 157–167.
54. Sevrioukova, I.F., J.T. Hazzard, G. Tollin, and T.L. Poulos (2001). Laser flash induced electron transfer in P450cam monooxygenase: Putidaredoxin reductase-putidaredoxin interaction. *Biochemistry* **40**, 10592–10600.
55. Pochapsky, T.C., X.M. Ye, G. Ratnaswamy, and T.A. Lyons (1994). An NMR-derived model for the solution structure of oxidized putidaredoxin, a 2-Fe, 2-S ferredoxin from *Pseudomonas*. *Biochemistry* **33**, 6424–6432.
56. Nagano, S., H. Li, H. Shimizu, C. Nishida, H. Ogura, P.R. Ortiz de Montellano *et al.* (2003). Crystal structures of epothilone-D bound, epothilone-B bound, and substrate-free forms of cytochrome P450epoK. *J. Biol. Chem.* **278**, 44886–44893.
57. Tang, L., S. Shah, L. Chung, J. Carney, L. Kaz, C. Khosla *et al.* (2000). Cloning and heterologous expression of the epothilone gene cluster. *Science* **287**, 640–642.
58. Lee, D.-S., A. Yamada, H. Sugimoto, I. Matsunaga, H. Ogura, K. Ichihara *et al.* (2003). Substrate recognition and molecular mechanism of fatty acid hydroxylation by cytochrome P450 from *Bacillus subtilis*. *J. Biol. Chem.* **278**, 9761–9767.
59. Li, H. and T.L. Poulos (1997). The structure of the cytochrome p450BM-3 haem domain complexed with the fatty acid substrate, palmitoleic acid. *Nat. Struct. Biol.* **4**, 140–146.
60. Haines, D.C., D.R. Tomchick, M. Machius, and J.A. Peterson (2001). Pivotal role of water in the mechanism of P450BM-3. *Biochemistry* **40**, 13456–13465.
61. Modi, S., M.J. Sutcliffe, W.U. Primrose, L.Y. Lian, and G.C. Roberts (1996). The catalytic mechanism of cytochrome P450 BM3 involves a 6 Å movement of the bound substrate on reduction. *Nat. Struc. Biol.* **3**, 414–417.
62. Wester, M.R., E.F. Johnson, C. Marques-Soares, S. Dijols, P.M. Dansette, D. Mansuy (2003). The structure of mammalian cytochrome P450 2C5 complexed with diclofenac at 2.1 Å resolution: Evidence for an induced fit model of substrate binding. *Biochemistry* **42**, 9335–9345.
63. Wester, M.R., E.F. Johnson, C. Marques-Soares, P.M. Dansette, D. Mansuy, and C.D. Stout (2003, submitted). The structure of a substrate complex of mammalian cytochrome P450 2C5 at 2.3 Å resolution: Evidence for multiple substrate binding modes. *Biochemistry* **42**, 6370–6379.
64. Marques-Soares, C., S. Dijols, A. Macherey, M.R. Wester, E.F. Johnson, P.M. Dansette *et al.* (2003, submitted). Sulfaphenazole derivatives as tools for comparing cytochrome P450 2C5 and human cytochrome P450 2Cs: Identification of a new high affinity substrate common to those enzymes. *Biochemistry* **42**, 6363–6369.
65. Poulos, T.L., B.C. Finzel, and A.J. Howard (1986). Crystal structure of substrate-free *Pseudomonas putida* cytochrome P450. *Biochemistry* **25**, 5314–5322.
66. DiGleria, K., D.P. Nickerson, H.A.O. Hill, L.L. Wong, and V. Fulop (1998). Covalent attachment of an electroactive sulfhydryl reagent in the

active site of cytochrome P450cam as revealed by the crystal structure on the modified protein. *J. Am. Chem. Soc.* **120**, 46–52.

67. Dmochowski, I.J., B.R. Crane, J.J. Wilker, J.R. Winkler, and H.B. Gray (1999). Optical detection of cytochrome P450 by sensitizer-linked substrates. *Proc. Natl. Acad. Sci. USA* **9**, 12987–12990.
68. Dunn, A.R., A.M. Hays, D.B. Goodin, C.D. Stout, R. Chiu, J.R. Winkler *et al.* (2002). Fluorescent probes for Cytochrome P450 structural characterization and inhibitor screening. *J. Am. Chem. Soc.* **124**, 10254–10255.
69. Li, H. and T.L. Poulos (1995). Modeling protein substrate interactions in the heme domain of cytochrome P450BM-3. *Acta Crystallogr. D* **51**, 21–32.
70. Paulsen, M.D. and R.L. Ornstein (1995). Dramatic differences in the motions of the mouth of open and closed cytochrome P450BM-3 by molecular dynamics simulations. *Proteins* **21**, 237–243.
71. Park, S.Y., H. Shimizu, S. Adachi, A. Nakagawa, I. Tanaka, K. Nakahara *et al.* (1997). Crystal structure of nitric oxide reductase from denitrifying fungus *Fusarium oxysporum*. *Nat. Struc. Biol.* **4**, 827–832.
72. Zerbe, K., O. Pylypenko, F. Vitali, W. Zhang, S. Rouset, M. Heck *et al.* (2002). Crystal structure of OxyB, a cytochrome P450 implicated in an oxidative phenol coupling reaction during vancomycin biosynthesis. *J. Biol. Chem.* **277**, 47476–47485.
73. Podust, L., Y. Kim, M. Arase, B. Neely, B. Beck, H. Bach *et al.* (2003). The 1.92 A structure of *Streptomyces coelicolor* A3(2) Cyp154C1: A new monooxygenase that functionalizes macrolide ring systems. *J. Biol. Chem.* **278**, 12214–12221.
74. Podust, L.M., T.L. Poulos, and M.R. Waterman (2001). Crystal structure of cytochrome P450 14alpha-sterol demethylase (CYP51) from *Mycobacterium tuberculosis* in complex with azole inhibitors. *Proc. Natl. Acad. Sci. USA* **98**, 3068–3073.
75. Scott, E.E., Y.A. He, M.R. Wester, M.A. White, C.C. Chin, J.R. Halpert, E.F. Johnson, and D. Stout (2003). An open confirmation of mammalian cytochrome P450 2B4 at 1.6Å resolution. *Proc. Natl. Acad. Sci. USA* **100**, 13196–13201.
76. Winn, P.J., S.K. Lüdemann, R. Gauges, V. Lounnas, and R.C. Wade (2002). Comparison of the dynamics of substrate access channels in three cytochrome P450s reveals different opening mechanisms and a novel functional role for a buried arginine. *Proc. Natl. Acad. Sci. USA* **99**, 5361–5366.
77. Pochapsky, T., T.A. Lyons, S. Kazanis, T. Arakaki, and G. Ratnaswamy (1996). A structure-based model for cytochrome P450cam-putidaredoxin interactions. *Biochimie* **78**, 723–733.